Aerosol-Cloud-Radiation Interaction in the fvGCM – Preliminary Results with the Nenes and Seinfeld Aerosol-Activation Scheme

Y. C. Sud, G. K. Walker
Climate and Radiation Branch
Laboratory for Atmospheres

O U T L I N E

1. McRAS Algorithms
2. Aerosol – Activation Modules
   (a) Some well-used ones
   (b) Nenes and Seinfeld 2003
3. Cloud-Aerosol MIP & Fields Examined
4. ARM-SGP SCM results with NENES Scheme
5. Conclusions

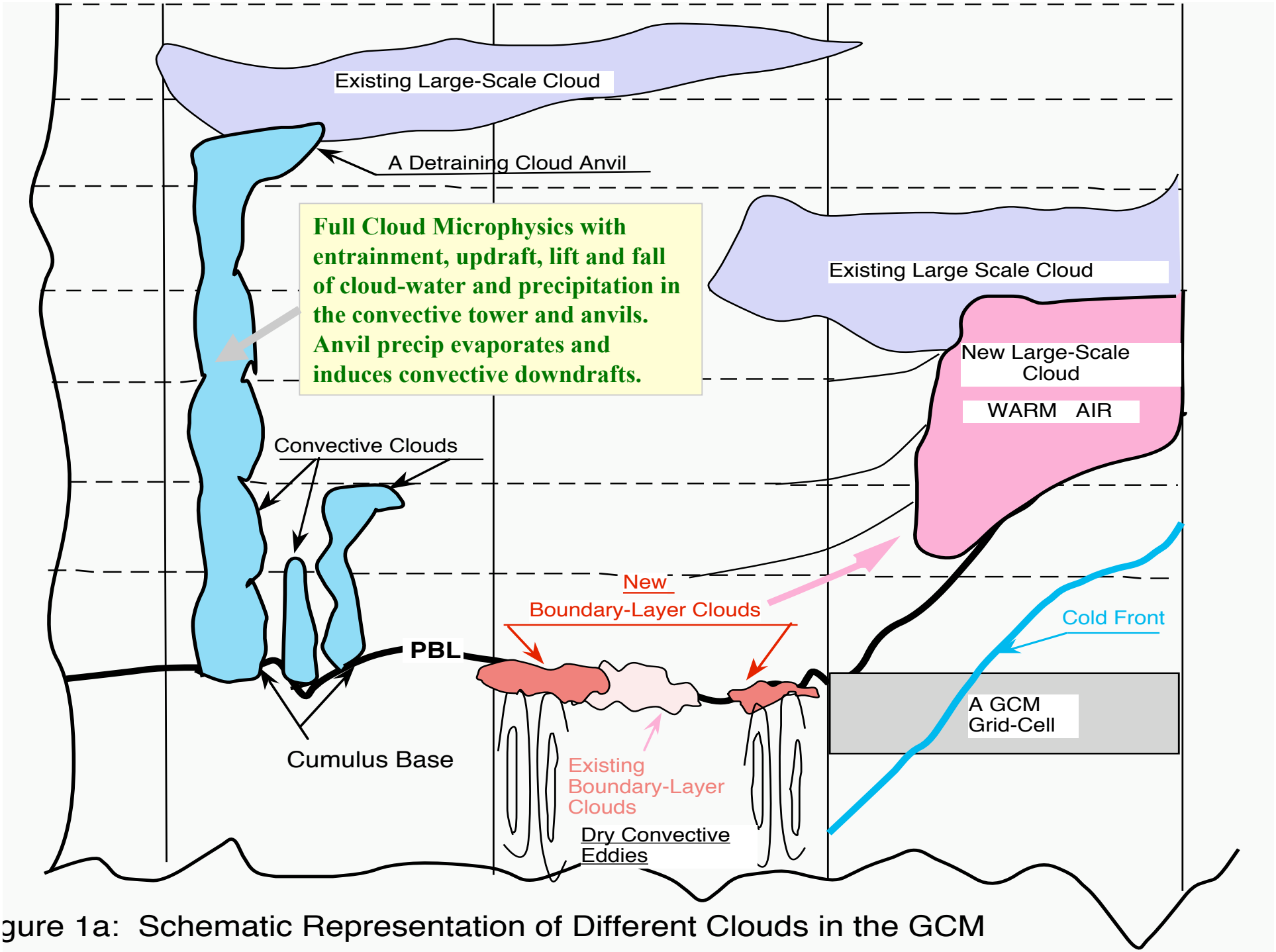

gure 1a: Schematic Representation of Different Clouds in the GCM

PBL-Clouds Parameterized on the moist convective Framework of Arakawa-Schubert

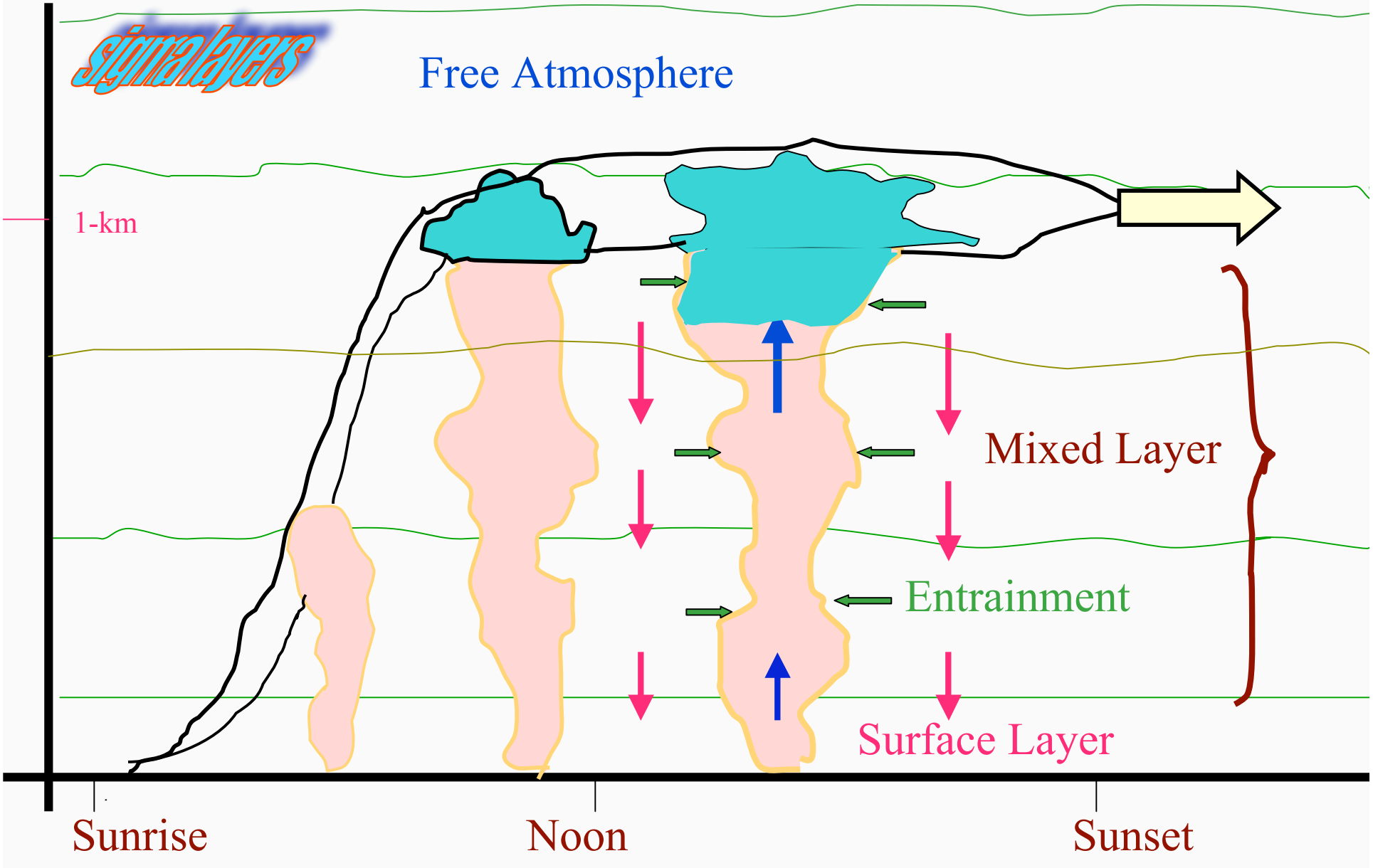

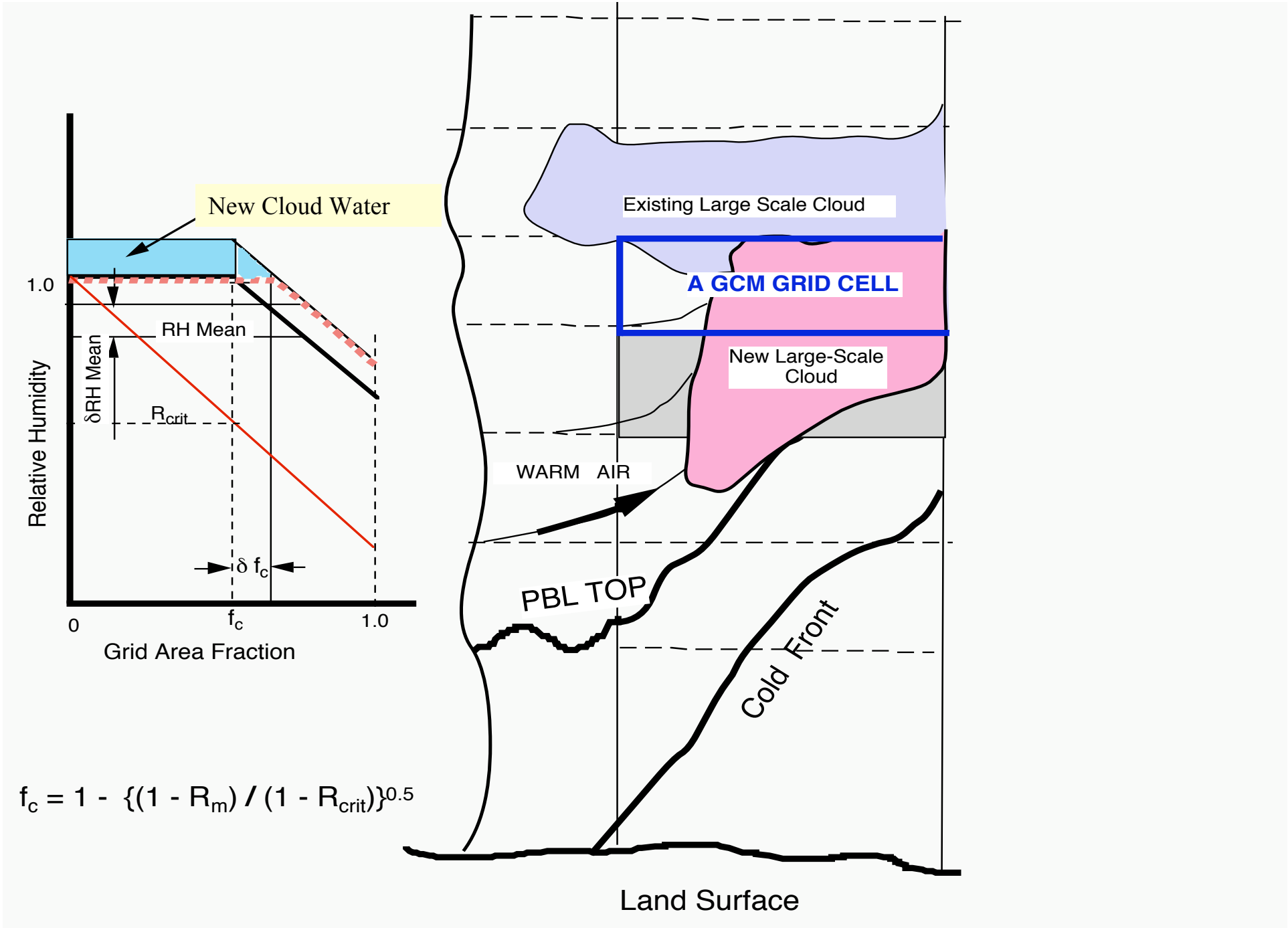

Figure 1C: Schematic Representation of Stratiform Clouds

Microphysics of Precipitation

Sundqvist (1988) fitted a function of specific cloud water substance ℓ_c, and auto conversion parameters ℓ_{crit}, and a time constant C_o. It is related to precipitation formation rate R_P through f_c. The equation is:

$$G_P = \frac{\ell_c f_c}{C_o}\left\{1 - \exp - \left(\frac{\ell_c}{\ell_{crit}}\right)^2\right\} = \ell_c R_P$$

Several scientists (e.g., LeTreut and Li, 1988; Tiedtke, 1993; Del Genio et al., 1996; and Zhao and Carr, 1997) have used this equation, but there are modifications. For example, Tiedtke (1993) uses a different formulation for high clouds with precipitating ice crystals; Del Genio et al. (1996) alters the exponent and includes the influence of collection of cloud water separately. We have been improving it with systematic evaluation experiments in SCMs using observational data such as ARM-CART (SGP).

TABLE-2
(Sud and Walker, 1999a)

Microphysical Parameters for Radiation

PARAMETER	UNITS	V A L U E S	
Symbol (s)		Land	Ocean
Effective rad., r_e, (water)	(mm)	7.0	10.0
Number Density, N (water)	(# cm-3)	170.0	60.0
Effective rad., r_e, (ice)*	(mm)	25.0	25.0
Number Density, N (ice)*	(# cm-3)	0.06	0.06

* also from Ou and Liou (1995) & Moss et al. (1996). See Fig. 2b for details.

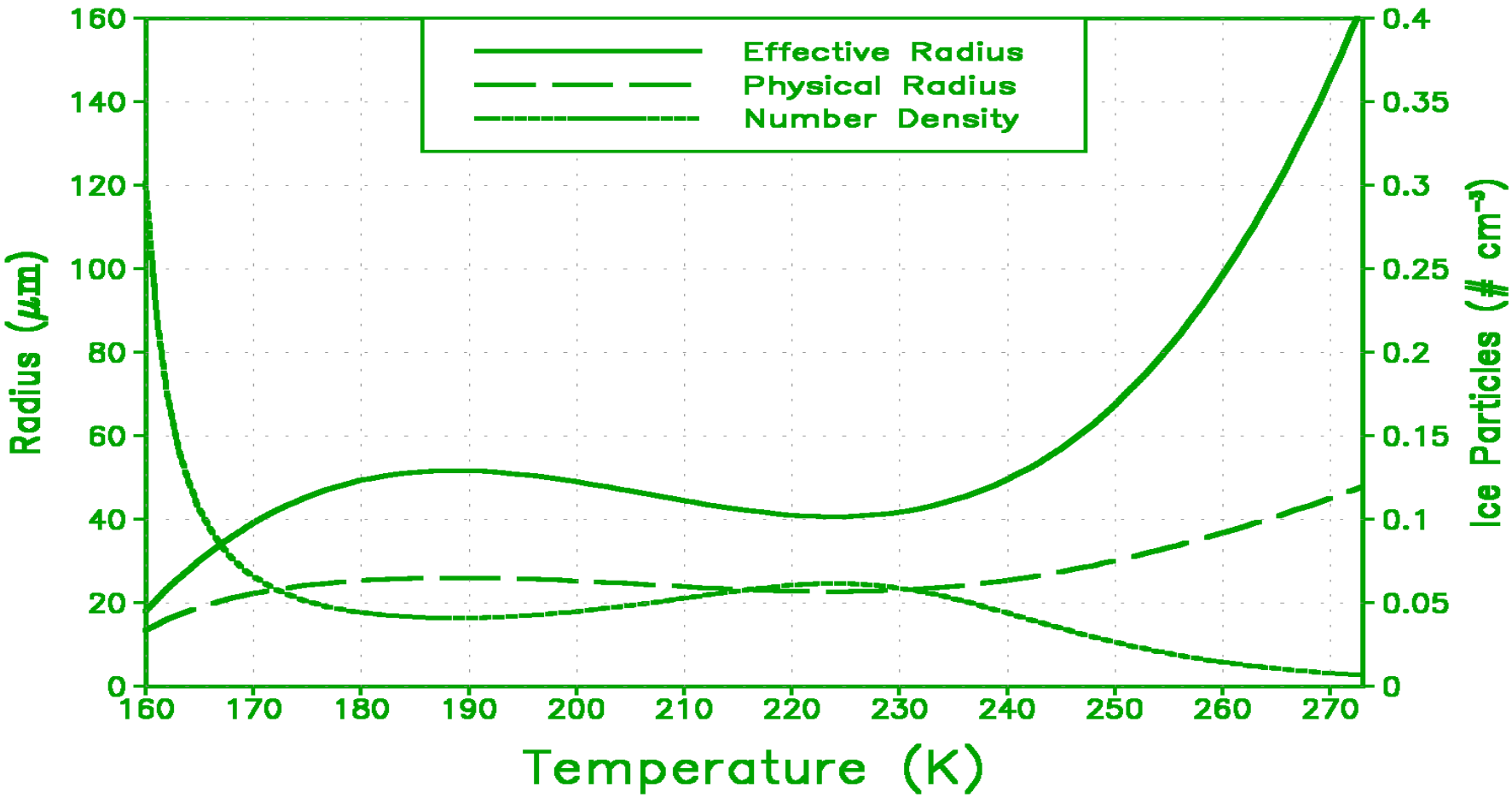

Cloud-ice effective and Physical radius as a function of temperature following Oh and Liou (1995) and Moss and Johnson (1995) as implemented in McRAS (Sud and Walker, 1999). Number density is a mere calculation for cloud-water substance mixing ratio of 5mg/Kg.

Vast differences in TOA-OLR showed its importance vividly!!!

Microcosm of "Big-Bang" of Precipitation : Cloud-water to Raindrops Microphysics

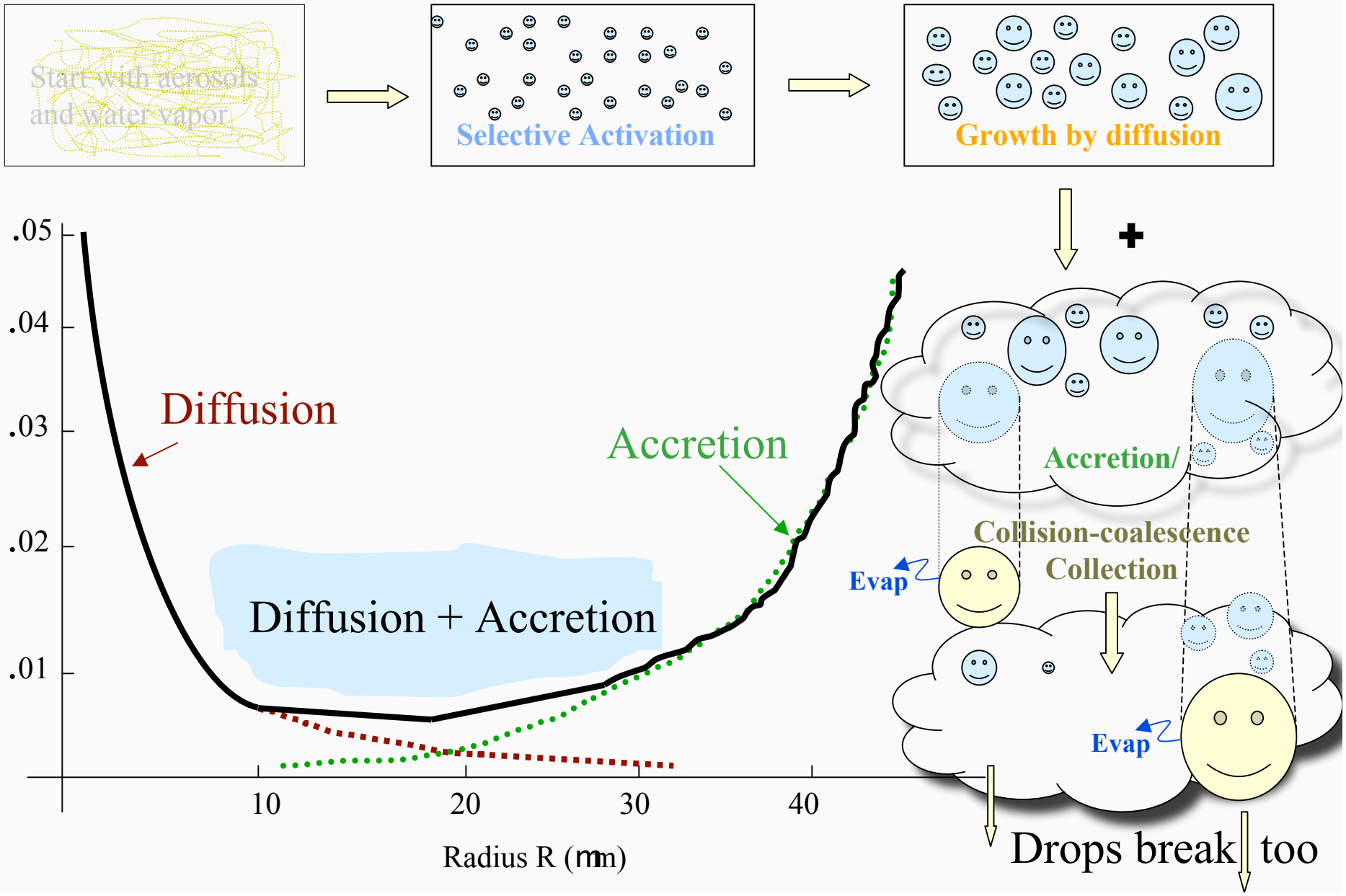

Properties affecting Droplet Growth

Köhler equation

Sfc tension *Molecular wt.*

$$S_{eq} \sim \left[\underbrace{\frac{2 M_w \sigma_s}{RT \rho_w r}} - \underbrace{\frac{3 M_w \cdot m_{solute}}{4\partial r^3 \tilde{n}_w M_{solute}} \cdot \text{íÖ}} \right]$$

Kelvin term A/r *Solute term* B / r^3

Van't Hoff factor

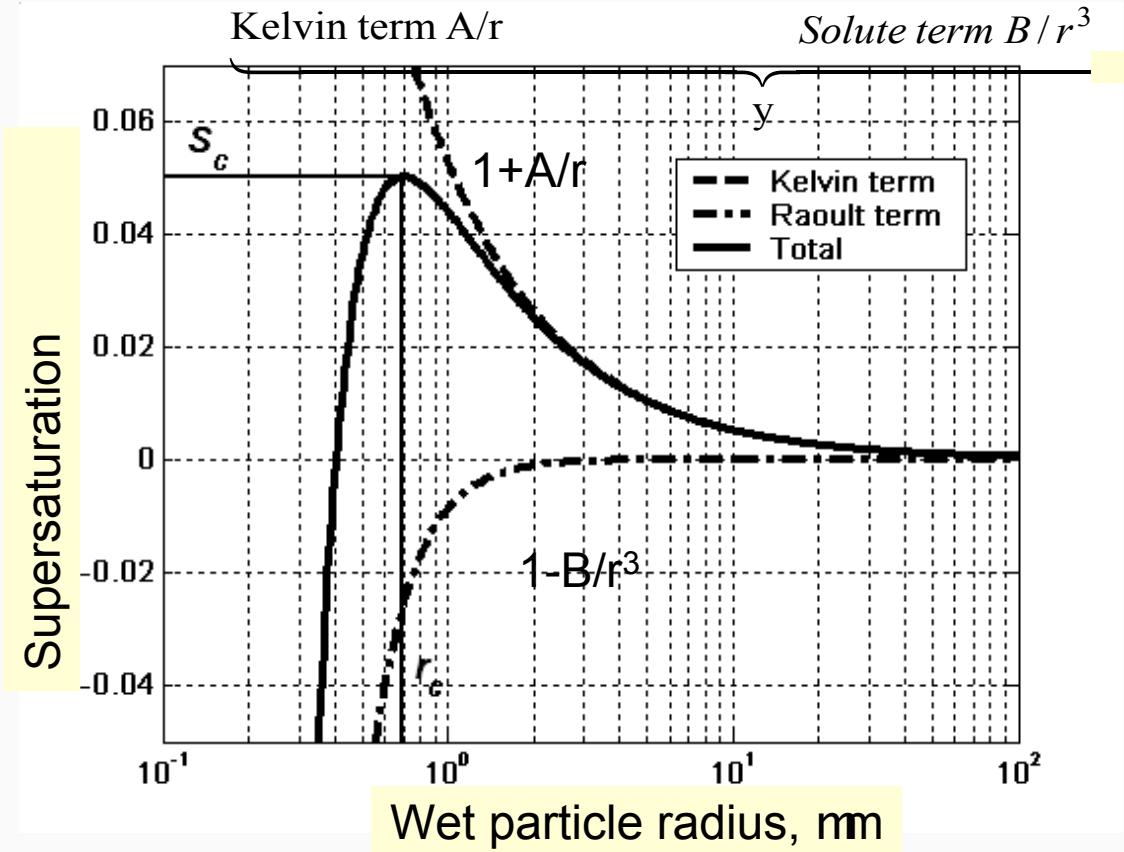

Particles are 'activated' if $S \geq S_c$

O U T L I N E

1. McRAS Algorithms
2. Aerosol – Activation Modules
   (a) Some well-used ones
   (b) Nenes and Seinfeld 2003
3. Cloud-Aerosol MIP & Fields Examined
4. ARM-SGP SCM results with NENES Scheme
5. Conclusions

Khairoutdinov & Kogan (2000) An End-to-End Bulk Parameterizations for Marine LES Model

I. **CCN Activation and Regeneration (in-cloud)**

a) $n_a = CS^k$ (Towmey, 1959 ; text book stuff , e.g., K & W, 1999),

b) $n_a = (n + N_c)\left(S/S_{max}\right)^k$, which gives

$$\left(\frac{\partial N_c}{\partial t}\right)_{actv} = \frac{\max\left\{0,\ (n + N_c)\min\left(1,\ \left(S/S_{max}\right)^k - N_c\right)\right\}}{\Delta t},$$

c) $$\frac{\partial q_c}{\partial t} = \frac{4\pi\rho_w}{3\rho_a} r_{act}^3 \left(\frac{\partial N_c}{\partial t}\right)_{actv}; \quad \text{assume } r_{act} = 1.0\ \mu m$$

Some Other well-known Schemes in GCMs

Ulrike Lohmann "On Cloud Nucleation and Cloud Droplets"

The number concentration of nucleated cloud droplets N_d is parameterized as a function of the aerosol number (or mass) concentration N_a and lately also in terms of the vertical velocity w, e.g.:

$$\mathbf{N_d = w\, N_a /(w + c_1\, N_a),}$$

where c_1 is a parameter that depends on the aerosol composition (Ghan et al., 1993; Lin and Leaitch

The autoconversion rate *(precipitation formation rate in clouds with no ice)* as a function of cloud water content q_l and N_d:

$$\mathbf{Q_{aut} \sim q_l^{\,a}\, N_d^{\,b}}$$

e.g. a=2.47, b=-1.79 (Khairoutdinov and Kogan, 2000)

a=4.7, b=-3.3 (Beheng, 1994)

Well-Known Schemes in GCMs - continued

Menon et al. GISS GCM:

$$CDNC_{Land} = 298 \times \log_{10} Na_{Land} - 595$$
$$CDNC_{Ocean} = 162 \times \log_{10} Na_{Ocean} - 273$$

Gultepe and Isaac (2001)

$$Na = \frac{\frac{ms}{\rho s} / r_s^3 + \frac{moc}{\rho oc} / r_{oc}^3 + \frac{mbc}{\rho bc} / r_{bc}^3}{4/3\pi}$$

Follow Lohmann et al. (1999) to go convert aerosol mass to aerosol number:
Density of Organic Carbon (OC) and Black Carbon (BC) = 1000 kg/m3
Sulfate =1769 kg /m3
Seasalt = 2000 kg/m3

Over ocean, add in Seasalt for sizes less than 2 mm (size is resolved).

r for land aerosol = 0.085 mm and r for ocean aerosol = 0.052 mm

Gultepe, I. and G.A. Isaac, Scale effects on averaging cloud droplet and aerosol number concentrations: observations and models, J. Climate, 12, 1268-1279, 2001.
Lohmann, U., J. Feichter, C.C. Chuang and J.E. Penner, Predicting the number of cloud droplets in the ECHAM GCM, J. Geophys. Res. 104, 9169-9198
Lohmann, U., Possible aerosol effects on ice clouds via contact nucleation, J. Atmos. Sci. 59, 647-656, 2002.

OUTLINE

1. McRAS Algorithms
2. Aerosol – Activation Modules
   (a) Some well-used ones
   (b) Nenes and Seinfeld 2003
3. Cloud-Aerosol MIP & Fields Examined
4. ARM-SGP SCM results with NENES Scheme
5. Conclusions

Implementation of the Standard Aerosol-Algorithms (Cloud-Aerosol MIP)

1. Algorithms Water Clouds: Sundqvist versus K&K (2000)

$$P_r = Com\left\{1 - \exp - \left(\frac{\ell_c}{\ell_{crit}}\right)^2\right\}; \quad Com/\ell_{crit} = C_o/\ell_o\ (f_1\ f_2\ f_3)\ \text{Sundqvist.}$$

$$P_r = 1350.*f_1\ f_2\ f_3 * \ell_c^{1.47} * N_d^{-1.79} \qquad \text{K \& K(2000).}$$

$$\text{where} \quad N_d = A\left(SO_4^{-2}\right)^B \quad \& \quad G_p = P_r\ell_c$$

2. Doctored Ice Clouds: Include Sulfate into Ou and Liou, 1995

$$M_{ice} = 4/3\pi\, r_{ice}^3\, \rho_{ice}\, N_{ice}; \quad (r_{ice}\ \text{Ou and Liou, 1995})$$

$$N_{ice} = f\left(SO_4\right)^B; \quad \text{Assume} \quad B = 1/3\ (\text{round number within}: 0.25/0.48)$$

$$\text{Obtain} \quad N_{ice}^{OL-Dctrd} = N_{ice}^{OL(1995)} * \left[\left(\overline{SO_4}\right)_{zm}/\left(SO_4\right)_{actual}\right]^{/9}$$

** $N_{ice}^{OL-Dctrd}$ is not to be used in future application(s)

Models and Datasets

1. AGCM: fvGCM also known as GEOS-4 GCM 2X2.5X32 sigma-layers.
2. NCAR-Physics but for McRAS Clouds (Sud & Walker, 1999 &2003) and Chou and Suarez (1998) Radiation.
3. **Sea-surface Temperatures**, vegetation cover, permanent snow and ice, and **sulfate-aerosols** are prescribed as monthly climatology, but are interpolated on Daily basis.
4. Everything else, e.g., soil moisture vegetation cover, cloud microphysics are prognostic and interactive.

GOCART-Model Sulfate-aerosol mass concentration Climatology

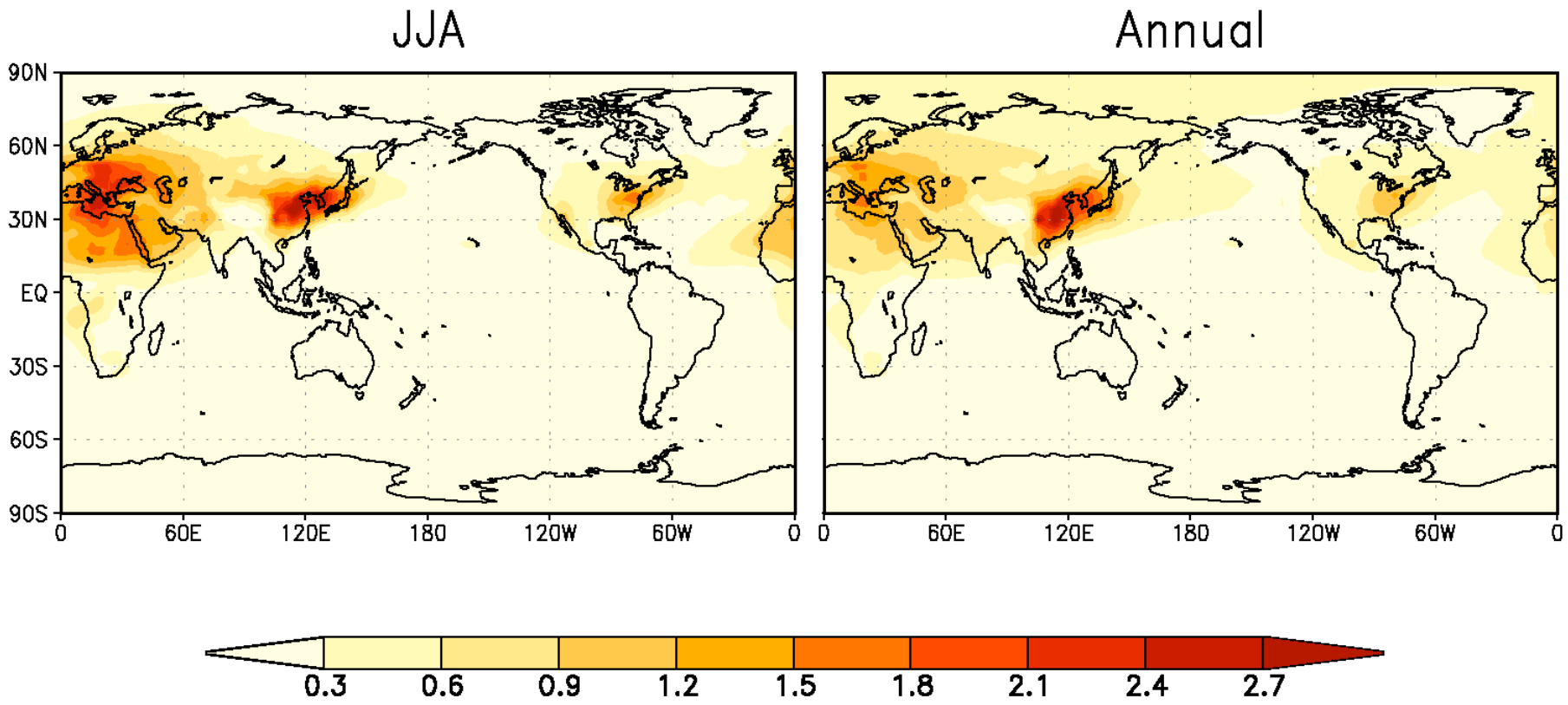

JJA: GOCART Sulfate Aerosol Optical Thickness

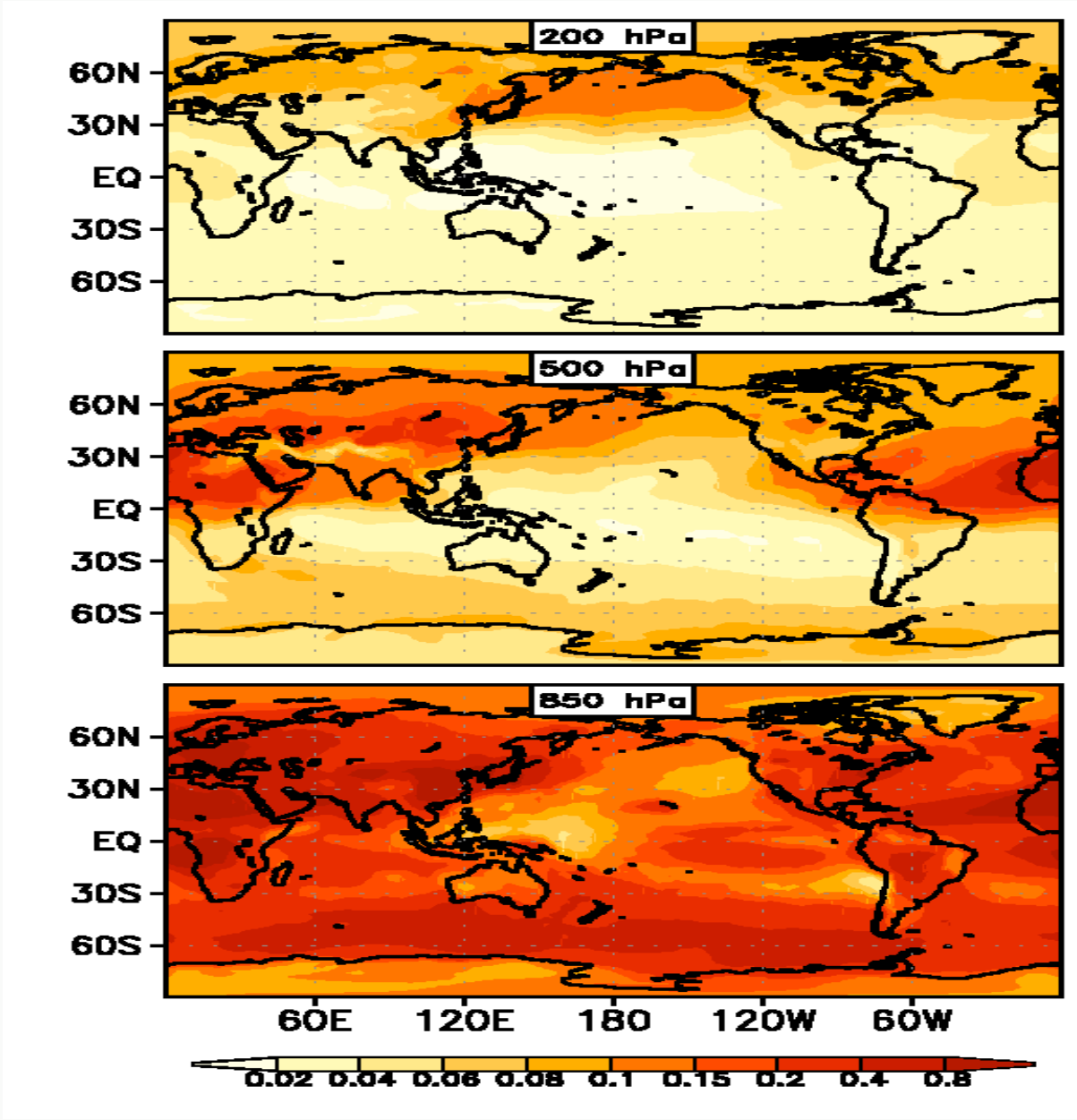

Design of the experiment

1. Initial Conditions are from a standard climatological SST run made with the fvGCM-NCAR physics; it is the atmospheric state on Sept 1, of year 47 of the simulation.
2. For adjustment to new formulation of aerosol-cloud interactions, we allow 4 month of adjustment and then analyze 5-years from Jan 1, yr 48 to Dec 31, yr 52
3. *The aerosol parameterization algorithms were designed for water clouds (below the freezing temperature) ; herein, even the ice-clouds have been modified/doctored to reflect the effect of sulfate-aerosols.*
4. Results are shown in the form of **SO4-Anomaly** minus **control** in the 5-year integration in which climatological SSTs, Vegetation Phenology and Morphology, permanent snow and ice are prescribed.

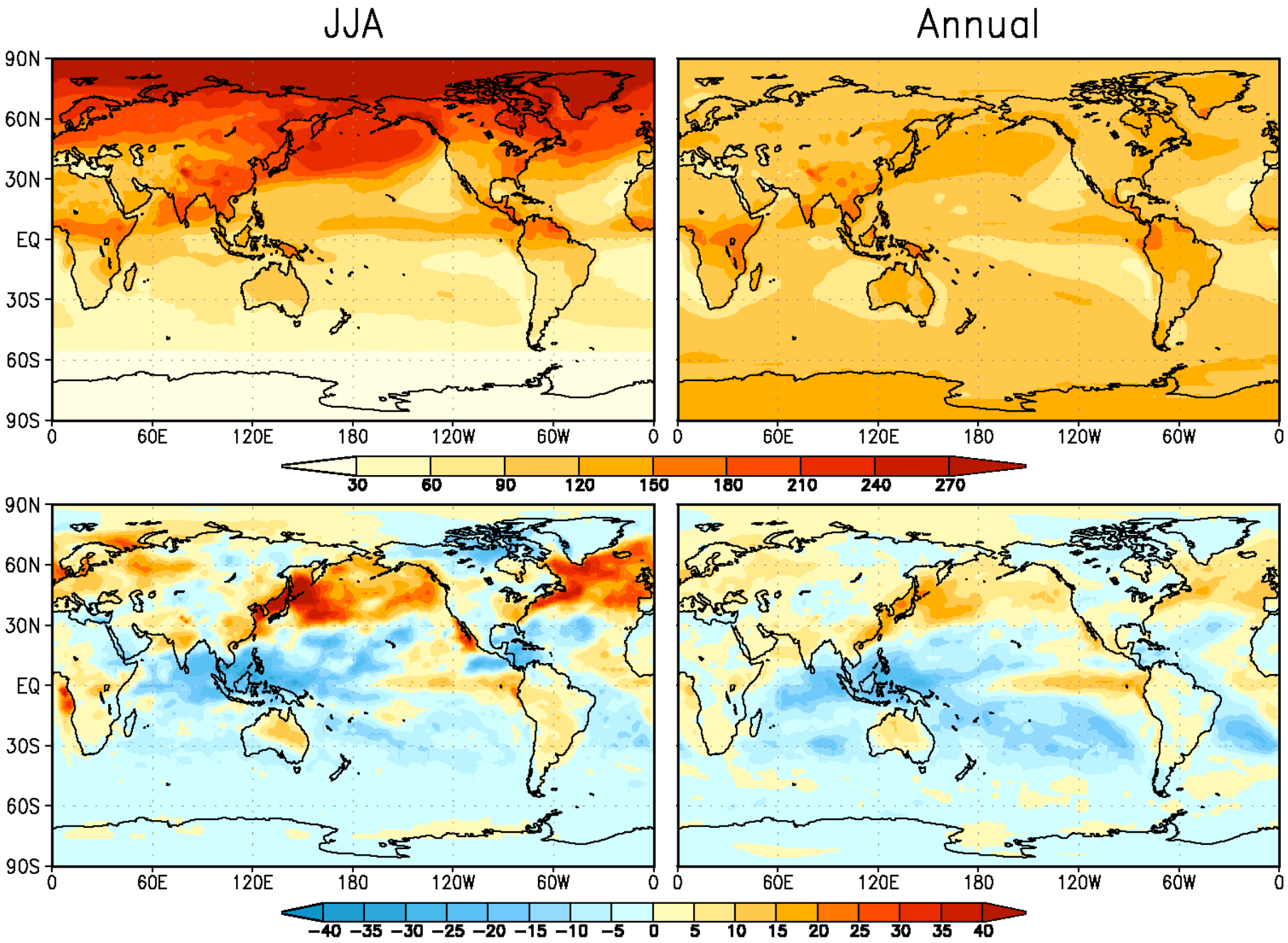

Outgoing shortwave radiation (W m^{-2}) (top) and difference from Control (bottom).

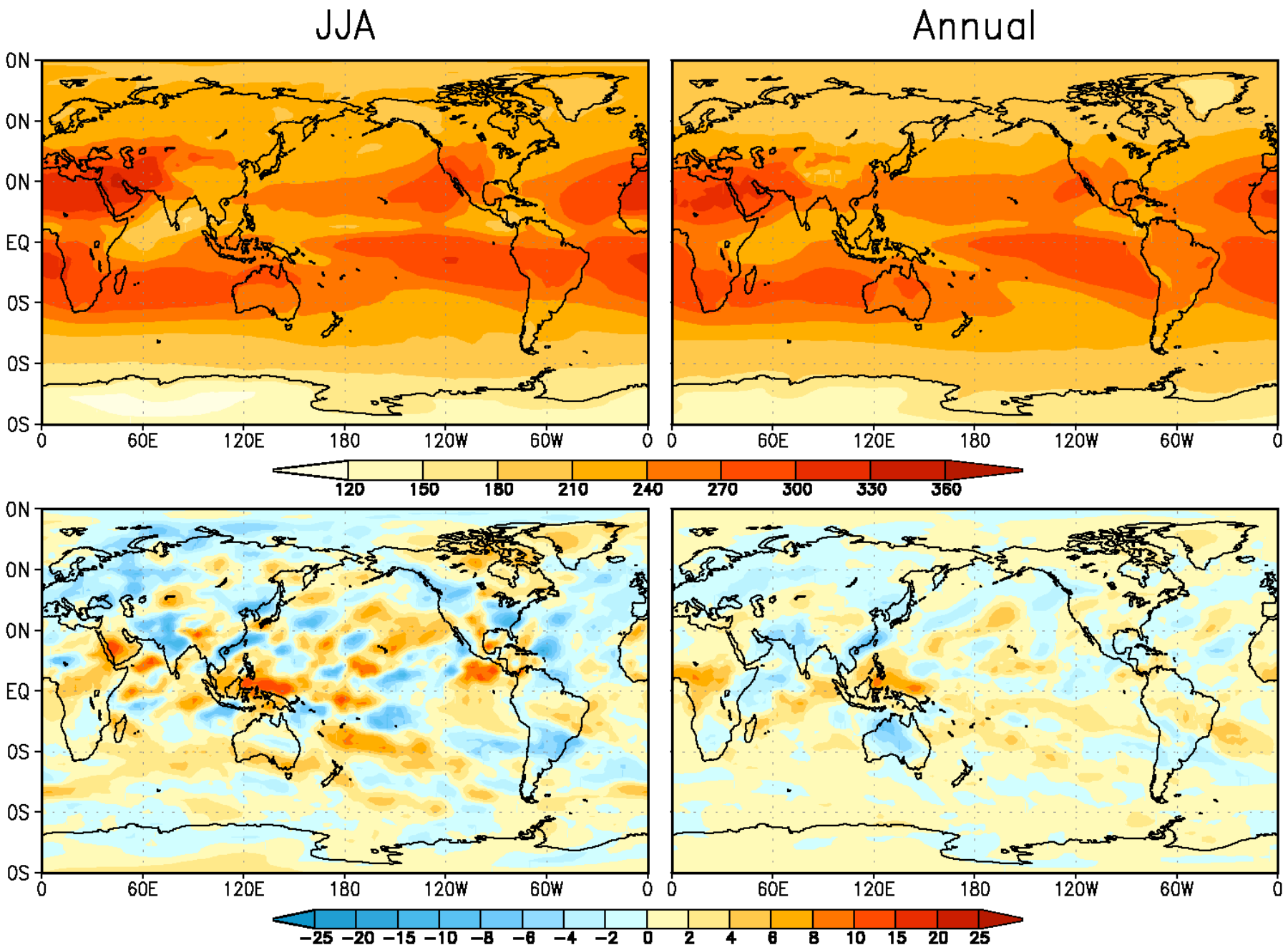

Outgoing longwave radiation (W m^{-2}) (top) and difference from Control (bottom).

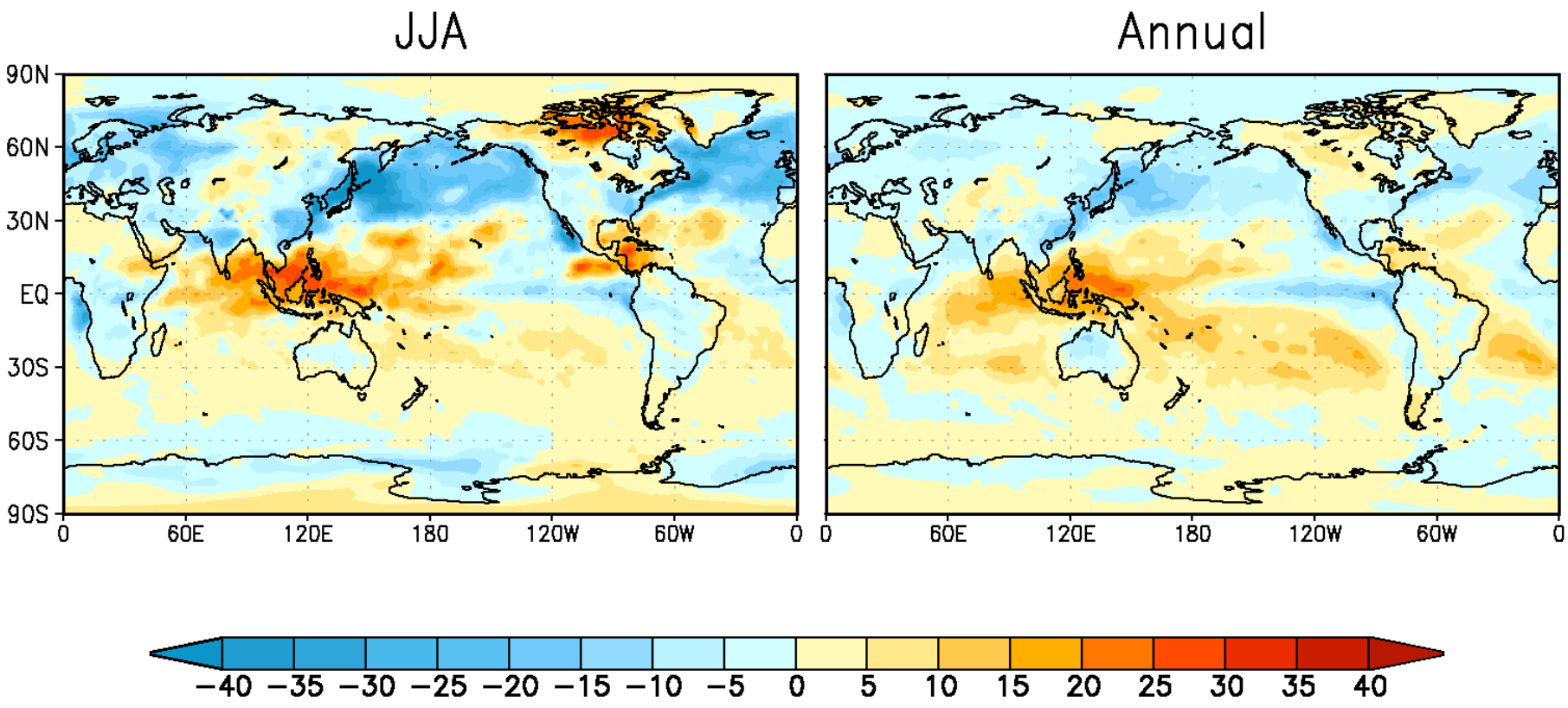

Surface net radiative forcing (W m^{-2}) difference from Control.

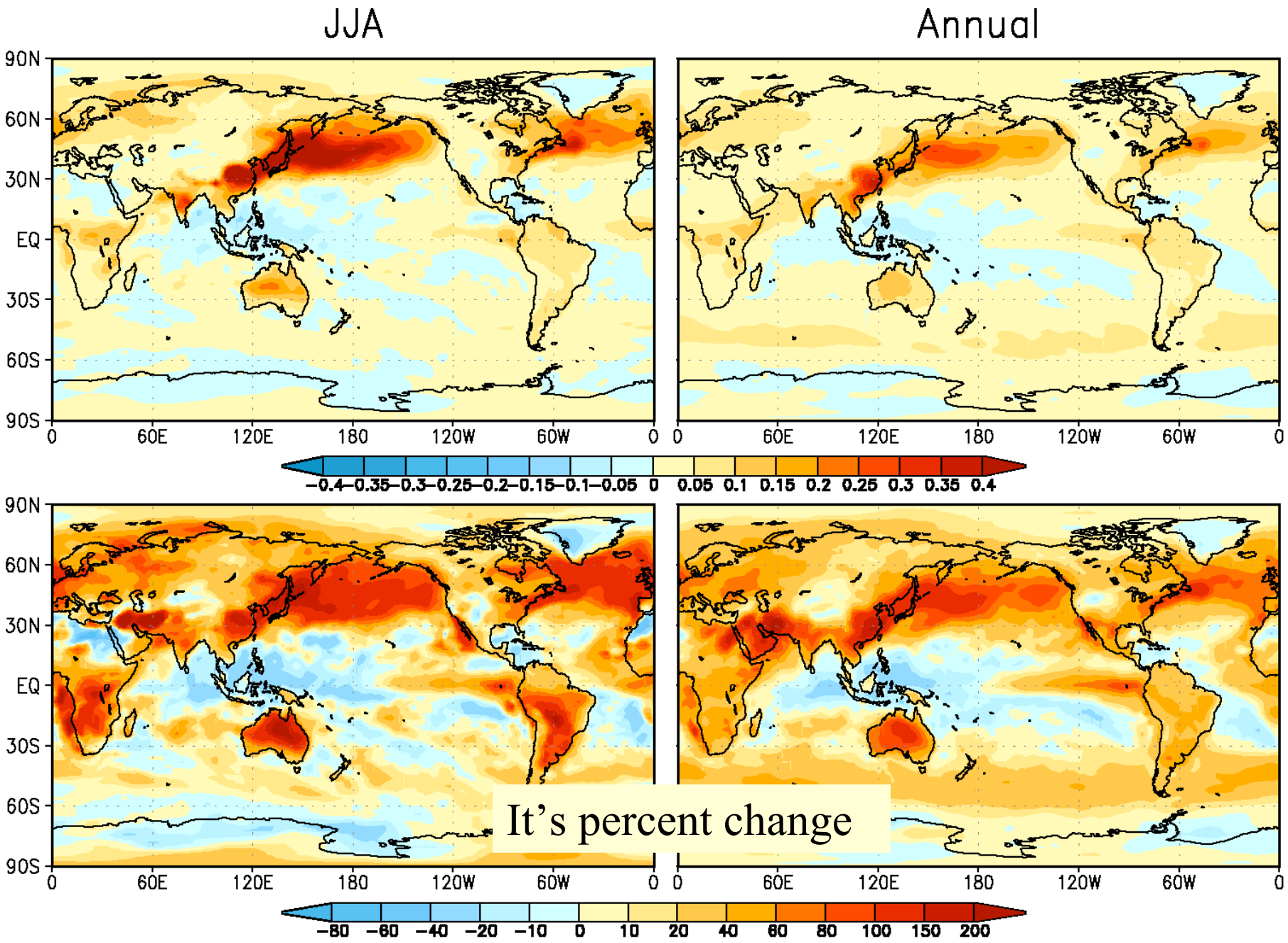

Column cloud water (kg m^{-2}) difference from Control (top) and percent difference (bottom)

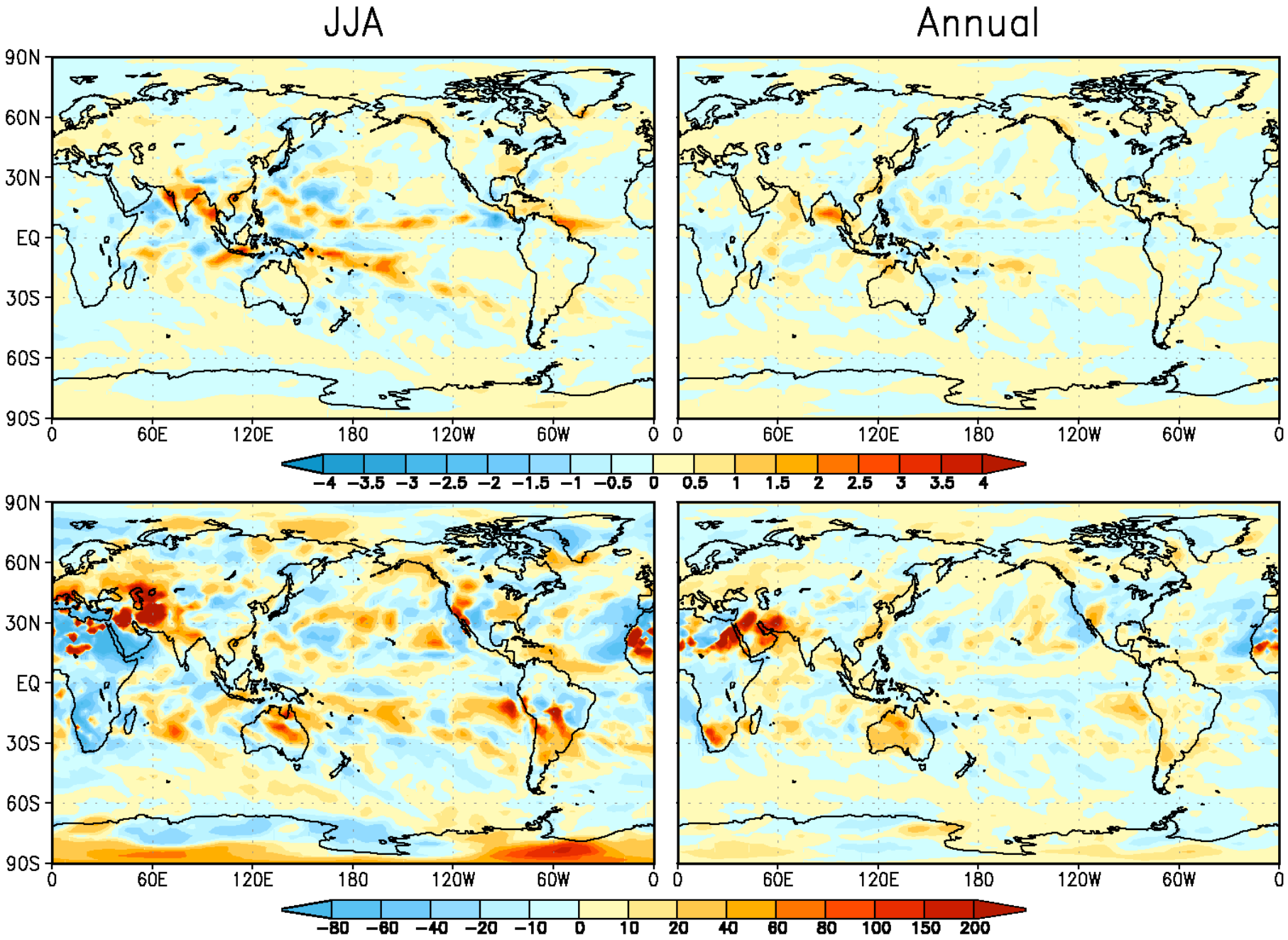

Precipitation (mm d^{-1}) difference from Control (top) and percent difference (bottom)

Sulfate Aerosol versus Cloud Water

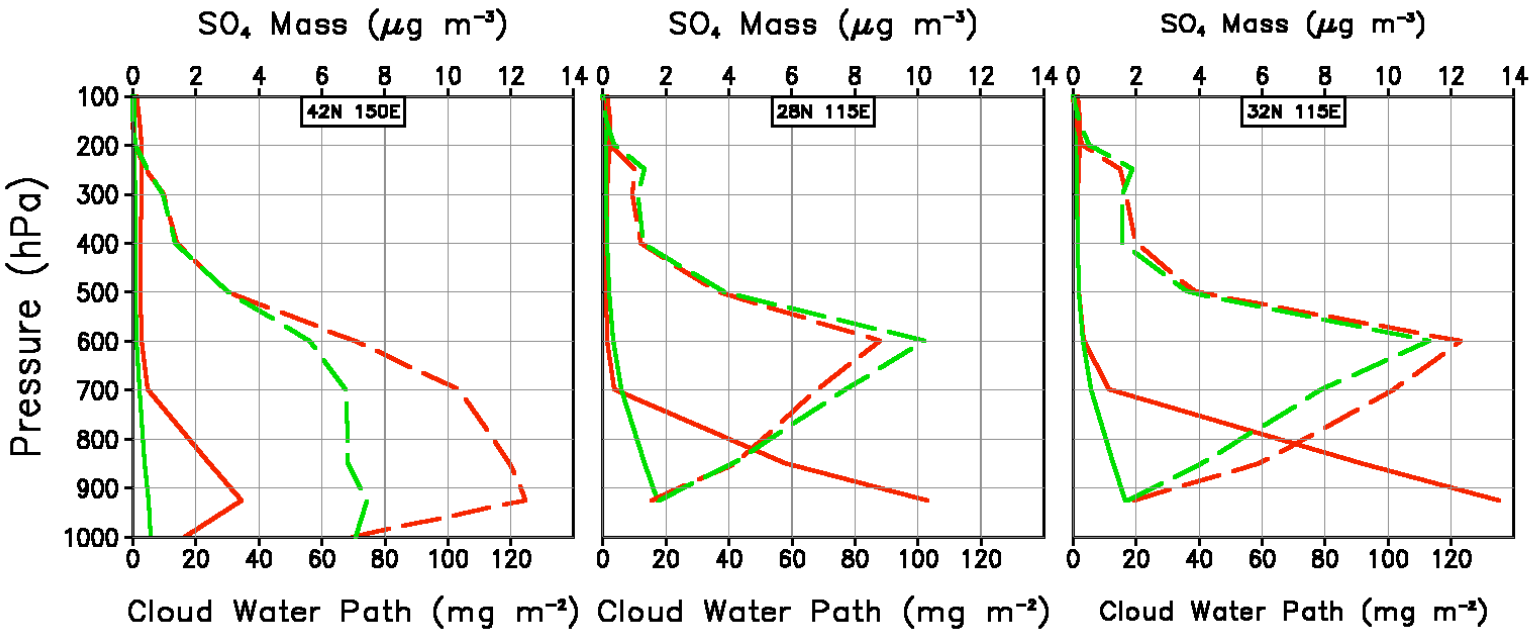

JJA mean cloud water path (mg m^{-2}) (dashed lines) and sulfate mass loading (μg m^{-3}) (solid lines) for selected locations. Red lines represents realistic sulfate distribution (Chin, YEAR), while green line represents simulation with global mean sulfate distribution. fvGCM with McRAS was used for the simulations.

Sulfates Data : Mian Chin; for the Year 2000

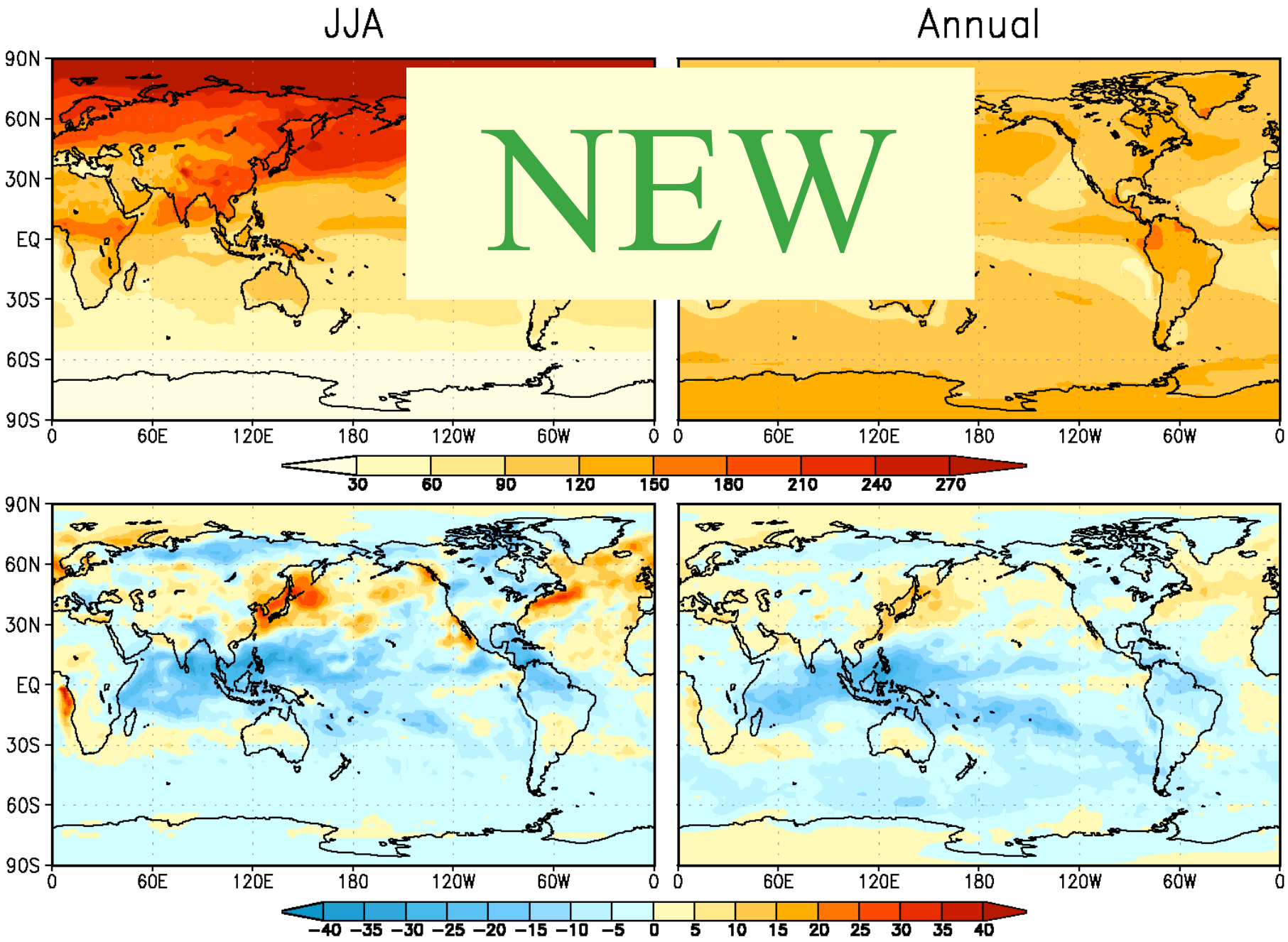

Outgoing shortwave radiation (W m^{-2}) (top) and difference from Control (bottom).

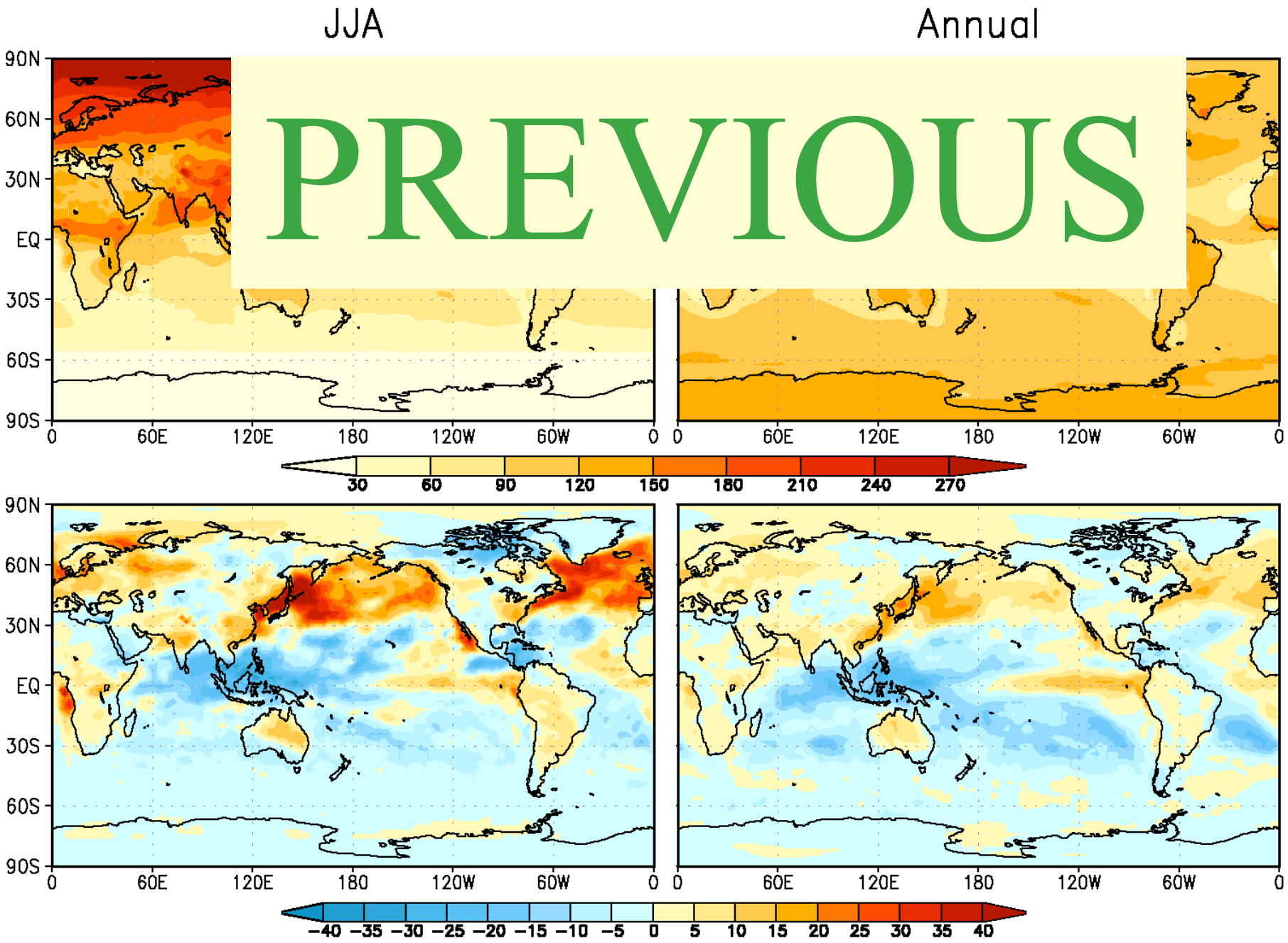

Outgoing shortwave radiation (W m^{-2}) (top) and difference from Control (bottom).

O U T L I N E

1. McRAS Algorithms
2. Aerosol – Activation Modules
   (a) Some well- used ones
   (b) Nenes and Seinfeld 2003
3. Cloud-Aerosol MIP & Fields Examined
4. ARM-SGP SCM results with NENES Scheme
5. Conclusions

2. Nenes and Seinfeld, 2003

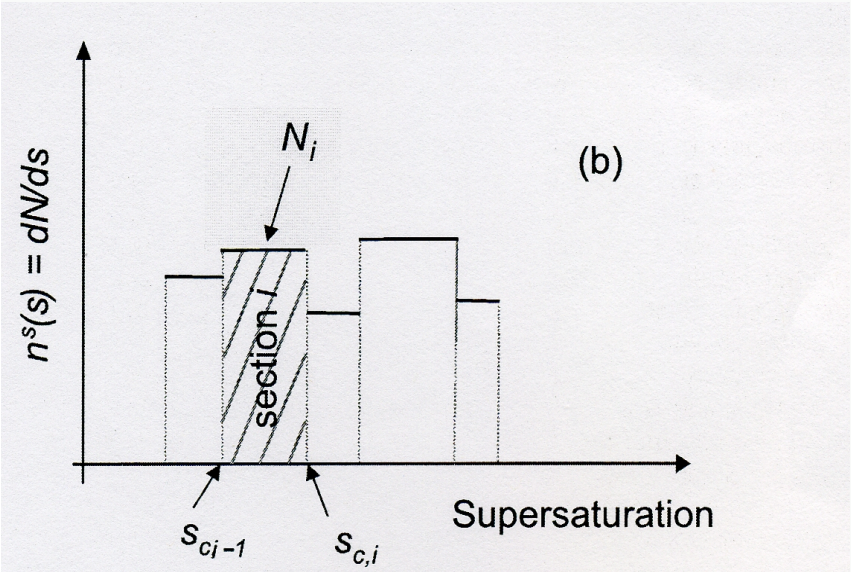

Figure 1. Illustration of the sectional representation of (a) aerosol number distribution, $n^d(D_p)$, and (b) supersaturation distribution, $n^s(D_p)$.

$$F^s(s) = \int_0^s n^s(s')ds' = \sum_{j=1}^{i-1} N_j + N_i\left(\frac{s - s_{c,i-1}}{s_{c,i} - s_{c,i-1}}\right), \qquad (6)$$

where i is the section that contains s and where $s_{c,0} = 0$.

[14] When k populations exist, the CCN spectrum is obtained by summing over all the aerosol populations:

$$F^s(s) = \sum_{l=1}^{k} \int_0^s n_l^s(s')ds'$$

$$= \sum_{l=1}^{k}\left[\sum_{j=1}^{i(l)-1} N_{j,l} + N_{i(l),l}\left(\frac{s - s^l_{c,i(l)-1}}{s^l_{c,i(l)} - s^l_{c,i(l)-1}}\right)\right], \qquad (7)$$

where $s^l_{c,i(l)-1}$ and $s^l_{c,i(l)}$ are the critical supersaturations for the boundaries of section i and population l that bound s. The variable $i(l)$ is used to indicate that each population l has its own section boundaries

3. Nenes and Seinfeld, 2003

4.1. Computation of Parcel Maximum Supersaturation

[18] In an adiabatic parcel the rate of change of the supersaturation, s, for a cloud parcel that ascends with a constant vertical velocity, V, is [*Pruppacher and Klett*, 1997; *Seinfeld and Pandis*, 1998]

supersaturation

$$\frac{ds}{dt} = \alpha V - \gamma \frac{dW}{dt}, \qquad (9)$$

Vertical velocity

Water Deposition

where

$$\alpha = \frac{gM_w\Delta H_v}{c_p RT^2} - \frac{gM_a}{RT}, \qquad \gamma = \frac{pM_a}{p^s M_w} - \frac{M_w \Delta H_v^2}{c_p RT^2} \qquad (10)$$

and where ΔH_v is the latent heat of condensation of water, T is the parcel temperature, M_w is the molecular weight of water, g is the acceleration of gravity, M_a is the molecular weight of air, c_p is the heat capacity of air, p^s is the water saturation vapor pressure, p is the ambient pressure, dW/dt is the rate of condensation of liquid water onto the drops, and R is the universal gas constant. The first term on the right hand side of equation (9) expresses the tendency of supersaturation to increase from the cooling of the parcel, while the second term expresses the tendency of super-
saturation to decrease because of depletion of water vapor

4. Nenes and Seinfeld, 2003

[19] The rate of water condensation on the droplet population can be expressed as

$$\frac{dW}{dt} = \frac{\pi}{2}\rho_w \int_0^s D_p^2 \frac{dD_p}{dt} n^s(s')ds', \tag{11}$$

where ρ_w is the density of water. By substituting equation (11) into equation (9), we obtain

$$\frac{ds}{dt} = \alpha V - \gamma \frac{\pi}{2}\rho_w \int_0^s D_p^2 \frac{dD_p}{dt} n^s(s')ds'. \tag{12}$$

[20] The parcel supersaturation reaches a maximum when water vapor availability from parcel cooling becomes equal to the depletion rate from the activated drops; this is expressed by setting ds/dt in equation (12) equal to zero:

$$\alpha V - \gamma \frac{\pi}{2}\rho_w \int_0^{s_{max}} D_p^2 \frac{dD_p}{dt} n^s(s')ds' = 0. \tag{13}$$

5. Nenes and Seinfeld, 2003

[23] One can integrate equation (16) from time τ, when the parcel supersaturation is equal to the CCN critical supersaturation, to the time of maximum supersaturation, $t_{\max}$, to give the droplet diameter at the time of $s_{\max}$:

$$D_p^2 = D_p^2(\tau) + 2\int_{\tau}^{t_{\max}} Gs\,dt. \tag{17}$$

[24] By substituting equations (17) and (16) into equation (13), we obtain

$$\frac{2\alpha V}{\pi\gamma\rho_w} - Gs_{\max}\int_0^{s_{\max}} \left(D_p^2(\tau) + 2G\int_{\tau}^{t_{max}} s\,dt\right)^{1/2} n^s(s')\,ds' = 0. \tag{18}$$

[25] Before proceeding further we need to evaluate the integral in equation (18), referred to hereinafter as $I(0, s_{max})$:

$$I(0, s_{max}) = G s_{max} \int_0^{s_{max}} \left(D_p^2(\tau) + 2G \int_\tau^{t_{max}} s dt \right)^{1/2} n^s(s') ds', \quad (19)$$

where the parameters in the parentheses indicate the limits of integration. If $I(0, s_{max})$ is evaluated and substituted into equation (18), the parcel maximum supersaturation can then be calculated, and a subsequent substitution into equation (8) would yield the cloud droplet number concentration.

4.2. Calculation of Integral *I*

[26] An analytical expression for I is not possible, but I has two asymptotic limits. The first limit, I_1, is obtained when

$$D_p^2(\tau) \ll 2G \int_\tau^{t_{max}} s dt. \quad (20)$$

7. Nenes and Seinfeld, 2003

In this limit the CCN experience significant growth beyond the point where they are exposed to $s > s_c$. Note that the above approximation is used to derive the parameterization of *Twomey* [1959]. The supersaturation integral in equation (19) can be evaluated using the lower bound of *Twomey* [1959]:

$$\int_{\tau}^{t_{\max}} s\,dt \approx \frac{1}{2\alpha V}\left(s_{\max}^2 - s(\tau)^2\right), \tag{21}$$

where $s(\tau)$ is the parcel supersaturation at time τ. Substituting equations (20), (21), and (5) into equation (19), we eventually obtain

$$I_1(0, s_{\max}) = \frac{s_{\max} G^{3/2}}{(aV)^{1/2}} ; \sum_{j=1}^{i} \frac{N_j}{s_c^j - s_c^{j-1}} \cdot \left[\frac{x}{2}\left(s_{\max}^2 - x^2\right)^{1/2} + \frac{s_{\max}^2}{2} \cdot \arcsin\frac{x}{s_{\max}}\right]_{x=s_c^{j-1}}^{x=s_c^j}, \tag{22}$$

where the bracket signifies the difference between evaluation at $x = s_c^j$ and $x = s_c^{j-1}$ and where i is the section that contains $s_{\max}$ (i.e., $s_c^{i-1} \le s_{\max} \le s_c^i$).

[27] The second limit, I_2, of I is obtained when

8. Nenes and Seinfeld, 2003

where the bracket signifies the difference between evaluation at $x = s_c^j$ and $x = s_c^{j-1}$ and where i is the section that contains s_{max} (i.e., $s_c^{i-1} \leq s_{max} \leq s_c^i$).

[27] The second limit, I_2, of I is obtained when

$$D_p^2(\tau) \gg 2G \int_\tau^t s\,dt, \tag{23}$$

$$I_2\left(s_c^1, s_{max}\right) = \frac{2Gs_{max}}{3}\left[\sum_{j=2}^{i-1}\left(\frac{N_j A_j}{s_c^j - s_c^{j-1}}\right)\right.$$

$$\left.\cdot \ln\frac{s_c^j}{s_c^{j-1}} + \left(\frac{N_i A_i}{s_c^i - s_c^{i-1}}\right)\ln\frac{s_{max}}{s_c^{j-1}}\right], \tag{24}$$

10. Nenes's Formulation, 2003

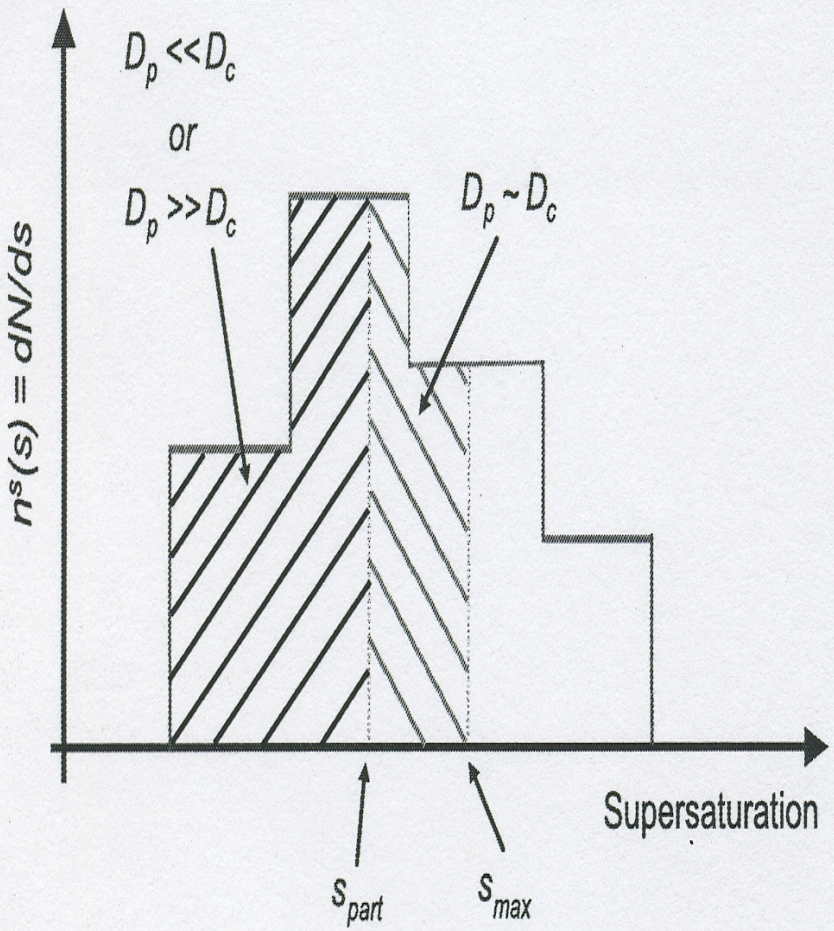

Figure 2. Illustration of the two subpopulations used in developing the parameterization.

4.3. Concept of "Population Splitting"

[28] While neither of equations (22) or (24) alone are expected to describe the behavior of all the CCN during their activation, it is reasonable to divide the CCN into two groups: those that would follow equation (22) and others that would follow equation (24). This classification of CCN, which we call "population splitting," will be used to approximate I:

$$I = I_1\left(0, s_{\text{part}}\right) + I_2\left(s_{\text{part}}, s_{\max}\right). \qquad (25)$$

[29] The ordering of the two integrals is deliberate: I_1 is used for low s_c CCN, while I_2 is used for the remaining CCN. This ordering will be justified subsequently (in section 4.4). The upper bound of I_1 and the lower bound of I_2 in equation (25) is termed the "partitioning critical supersaturation," s_{part} (Figure 2). Physically, this supersaturation defines two populations of droplets: one for which

11. Nenes Formulation, 2003

4.4. Implementation of Population Splitting

[30] Numerical simulations with a cloud parcel model [*Nenes et al.*, 2001] reveal that s_{part} depends on s_{max}, V, and the CCN spectrum characteristics. We will now attempt to derive theoretical expressions for s_{part}. An obvious candidate for s_{part} is the critical supersaturation of the CCN population, for which $D_p^2(\tau) = 2G\int_{\tau}^{t_{max}} s\,dt$. From equation (21) and substituting $D_p(\tau) = 2A/3s_{part}$, we obtain

$$\frac{4A^2}{9s_{part}^2} = \frac{G}{\alpha V}\left(s_{max}^2 - s_{part}^2\right), \tag{26}$$

where $A = 4M_w\sigma_w/RT\rho_w$ and σ_w is the surface tension of water. After some algebra, equation (26) leads to the quartic equation

$$p(s_{part}) = s_{part}^4 - s_{max}^2 s_{part}^2 + \frac{4A^2\alpha V}{9G} = 0. \tag{27}$$

[31] If the descriminant, $\Delta = s_{max}^4 - \frac{16A^2\alpha V}{9G}$, of $p(s_{part})$ is nonnegative, then equation (27) has two real roots with respect to s_{part}:

$$\left(\frac{s_{part,1}}{s_{max}}\right)^2 = \frac{1}{2}\left[1 - \left(1 - \frac{16A^2\alpha V}{9s_{max}^4 G}\right)^{1/2}\right];$$
$$\left(\frac{s_{part,2}}{s_{max}}\right)^2 = \frac{1}{2}\left[1 + \left(1 - \frac{16A^2\alpha V}{9s_{max}^4 G}\right)^{1/2}\right]. \tag{28}$$

[32] Each of the two roots, $s_{part1,2}$, expresses the s_c of those CCN for which their subsequent growth beyond activation is equal to D_c. These two characteristic s_c divide the CCN population into three groups: those with $s_c < s_{part,1}$, those with $s_{part,2} < s_c < s_{part,1}$, and those with $s_{part,2} < s_c$. If a CCN has an s_c between $s_{part,1}$ and $s_{part,2}$, then $p(s_c) < 0$, which means that the CCN experiences significant growth after it attains its critical diameter. For other values of s_c, $p(s_c) > 0$, which means that the growth experienced by the CCN is smaller than its critical diameter. Note that the latter

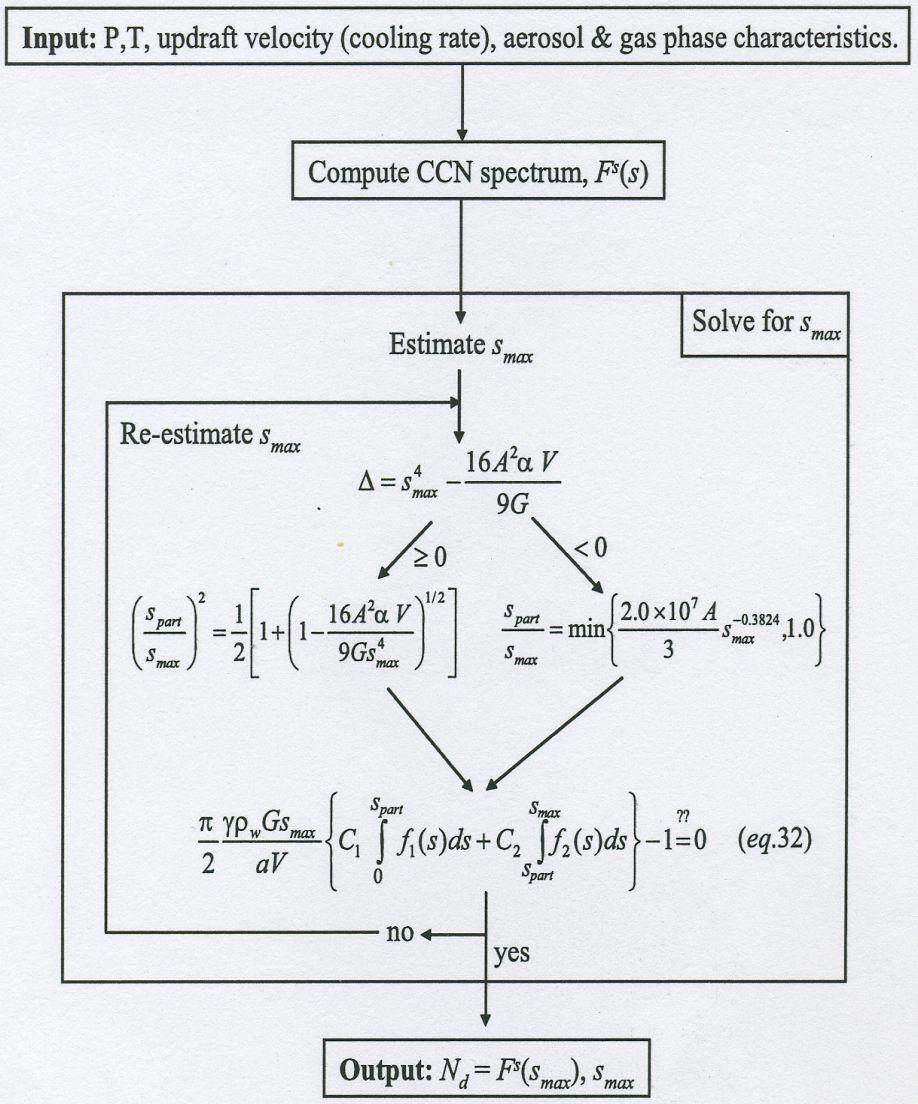

Figure 5. Parameterization algorithm.

OUTLINE

1. McRAS Algorithms
2. Aerosol – Activation Modules
   (a) Some well-used ones
   (b) Nenes and Seinfeld 2003
3. Cloud-Aerosol MIP & Fields Examined
4. ARM-SGP SCM results with NENES Scheme
5. Conclusions

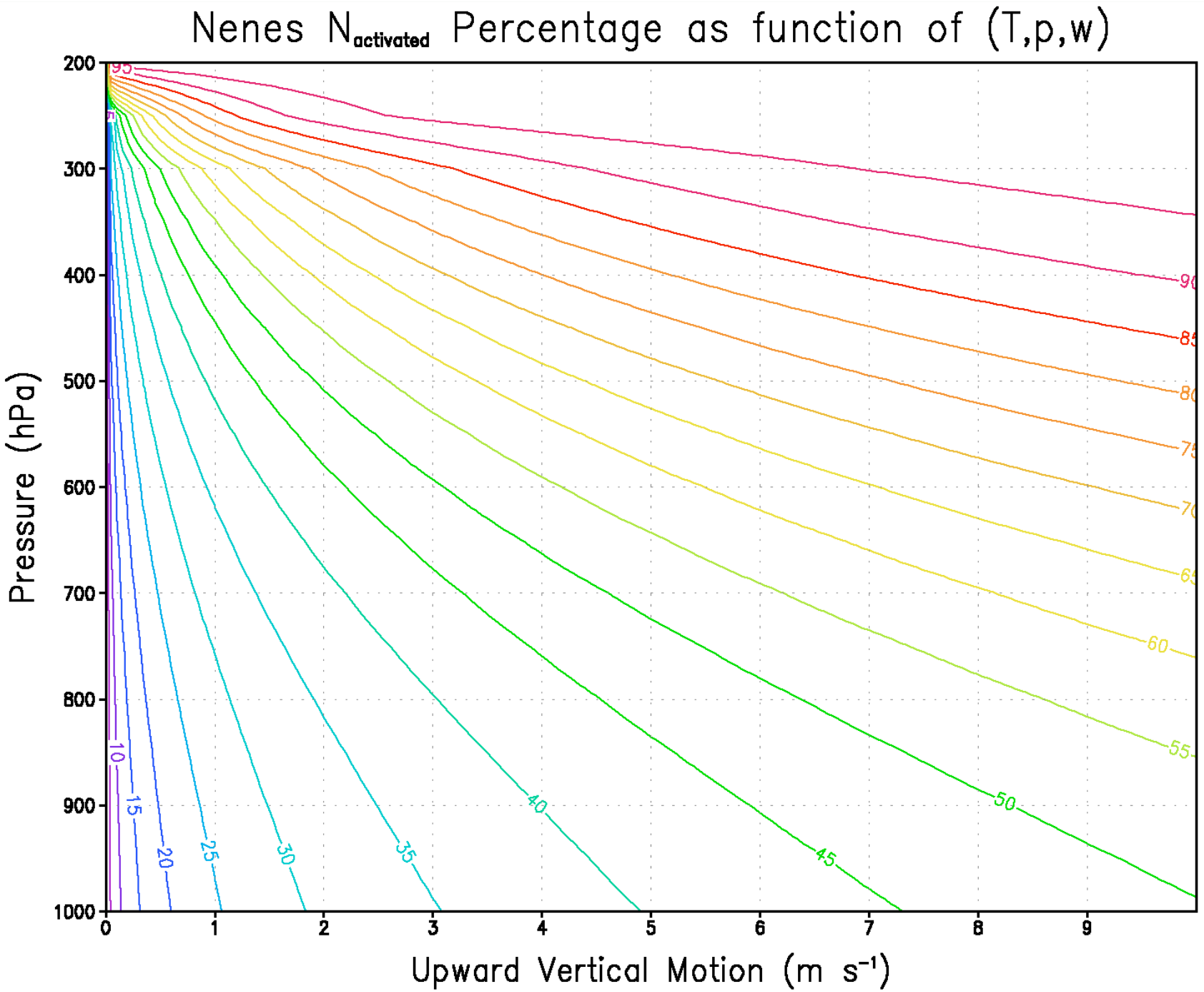
Nenes $N_{activated}$ Percentage as function of (T,p,w)
Pressure (hPa)
200
300
400
500
600
700
800
900
1000
0
1
2
3
4
5
6
7
8
9
Upward Vertical Motion (m s^{-1})
95
90
85
80
75
70
65
60
55
50
45
40
35
30
25
20
15
10
5

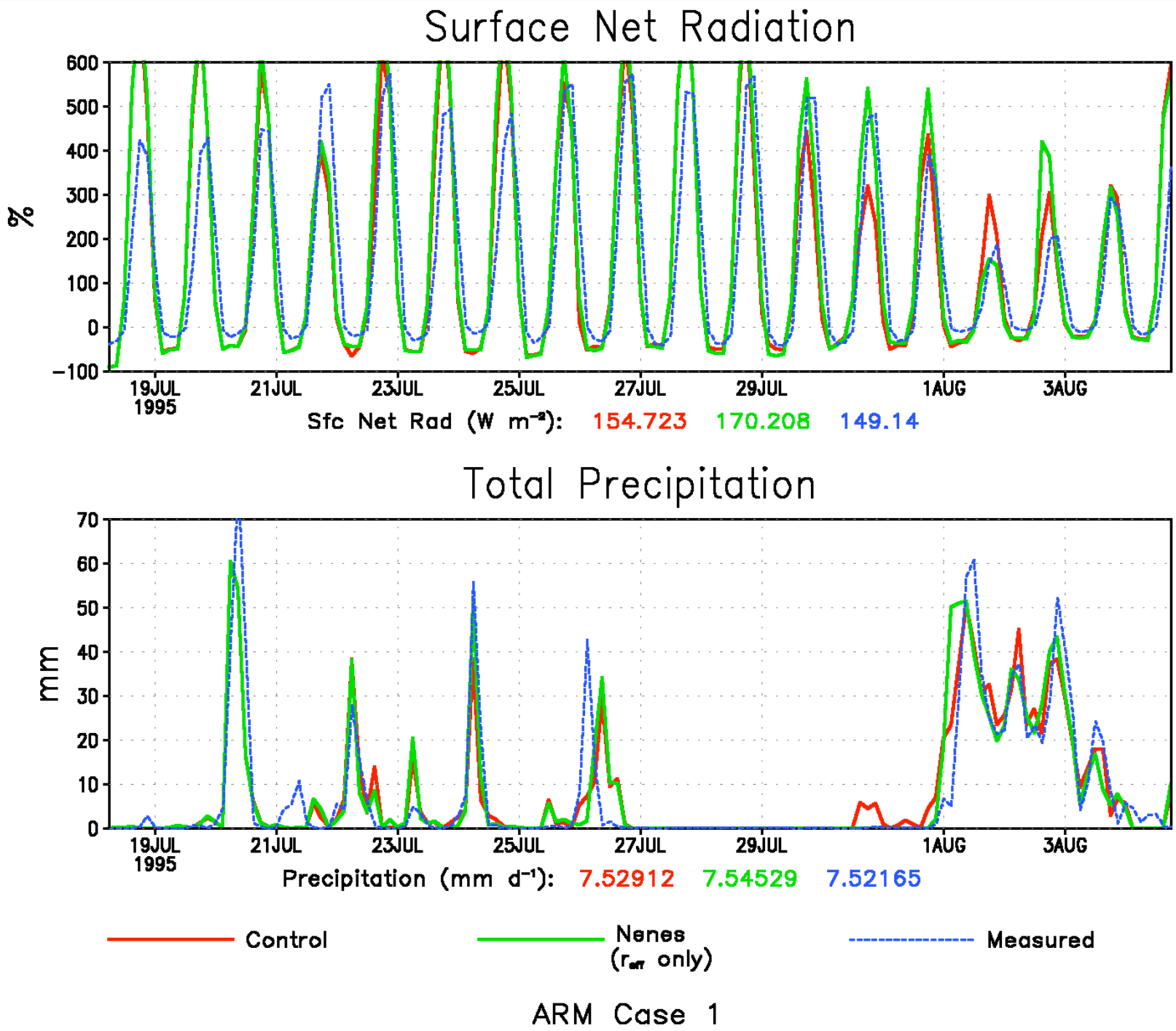
Surface Net Radiation
600
500
400
300
200
100
0
−100
%
19JUL
1995
21JUL
23JUL
25JUL
27JUL
29JUL
1AUG
3AUG
Sfc Net Rad (W m⁻²): 154.723 170.208 149.14
Total Precipitation
70
60
50
40
30
20
10
0
mm
19JUL
1995
21JUL
23JUL
25JUL
27JUL
29JUL
1AUG
3AUG
Precipitation (mm d⁻¹): 7.52912 7.54529 7.52165
Control
Nenes
(r_eff only)
Measured
ARM Case 1

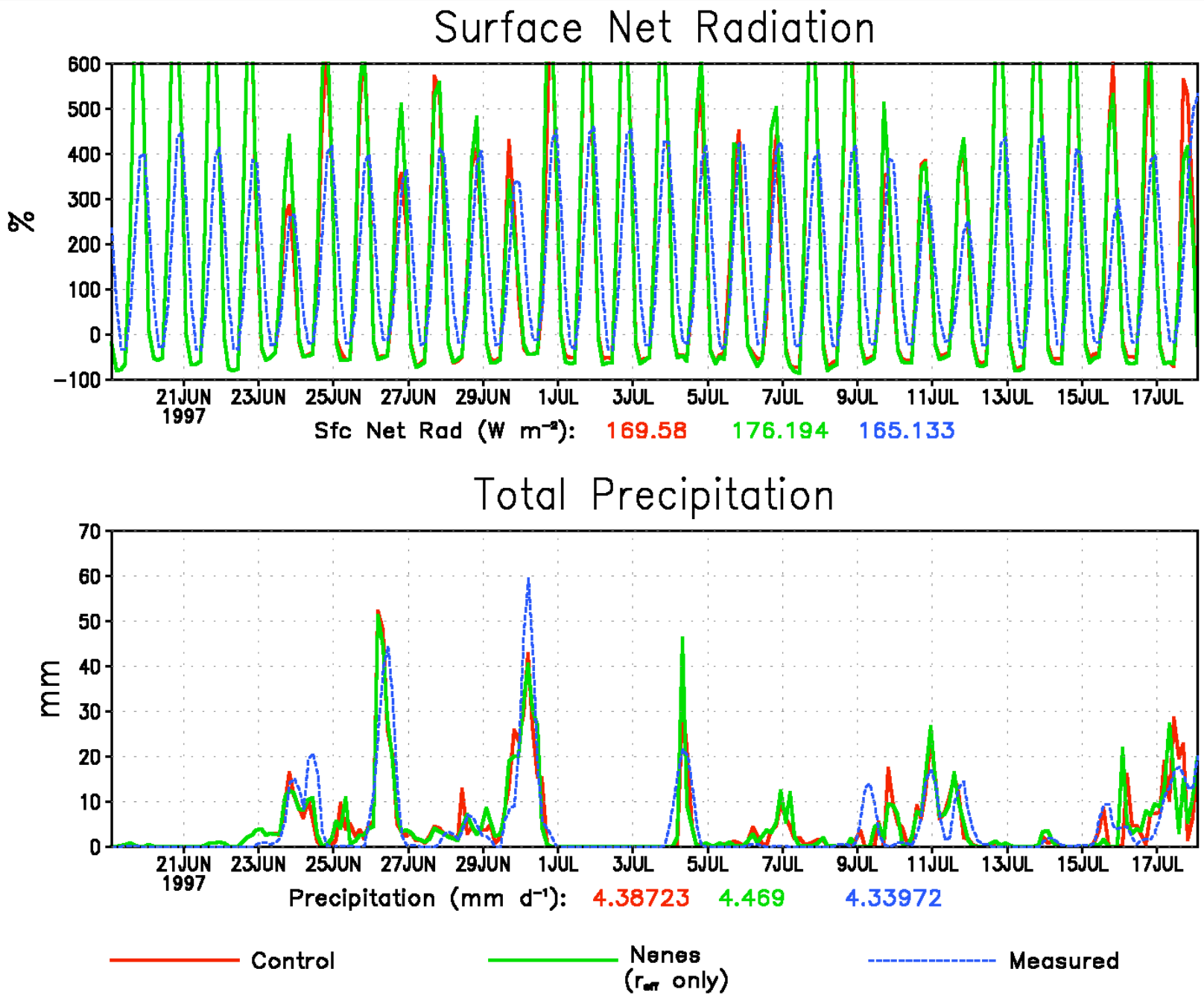
Surface Net Radiation
%
600
500
400
300
200
100
0
−100
21JUN 1997
23JUN
25JUN
27JUN
29JUN
1JUL
3JUL
5JUL
7JUL
9JUL
11JUL
13JUL
15JUL
17JUL
Sfc Net Rad (W m⁻²): 169.58 176.194 165.133
Total Precipitation
mm
70
60
50
40
30
20
10
0
21JUN 1997
23JUN
25JUN
27JUN
29JUN
1JUL
3JUL
5JUL
7JUL
9JUL
11JUL
13JUL
15JUL
17JUL
Precipitation (mm d⁻¹): 4.38723 4.469 4.33972
Control
Nenes (r_{air} only)
Measured
ARM Case 3

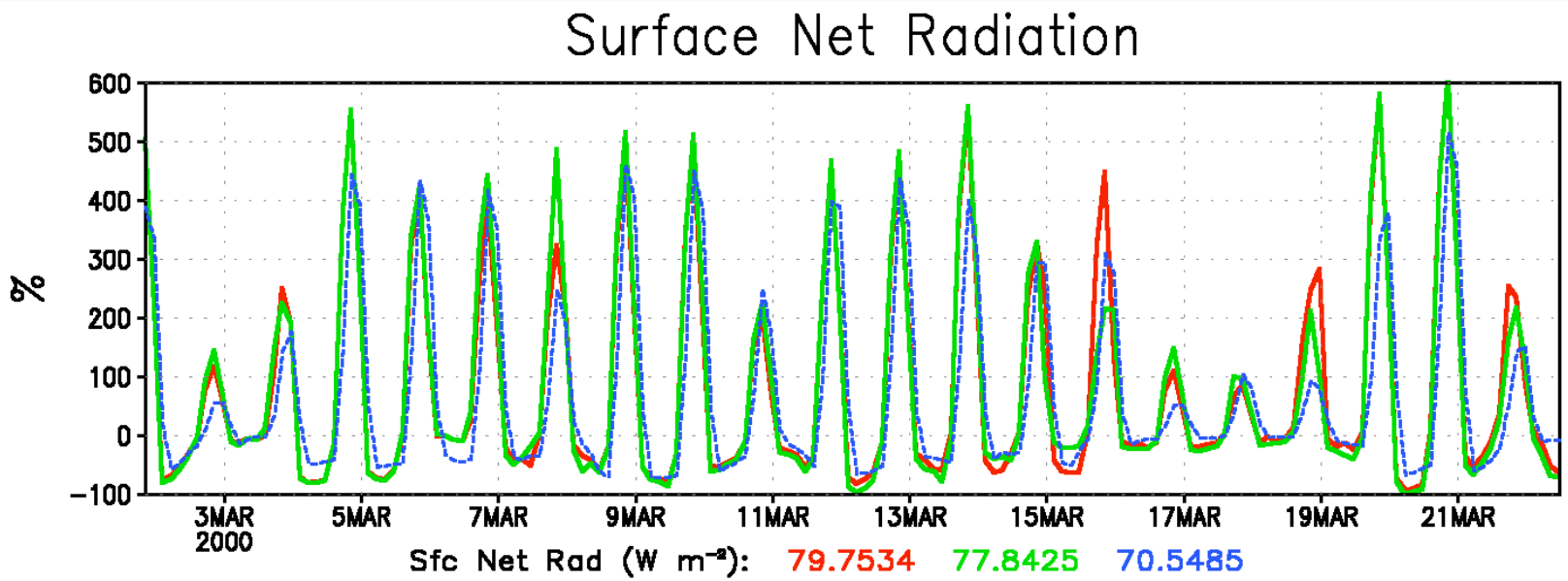
Surface Net Radiation
%
600
500
400
300
200
100
0
−100
3MAR
2000
5MAR
7MAR
9MAR
11MAR
13MAR
15MAR
17MAR
19MAR
21MAR
Sfc Net Rad (W m⁻²): 79.7534 77.8425 70.5485

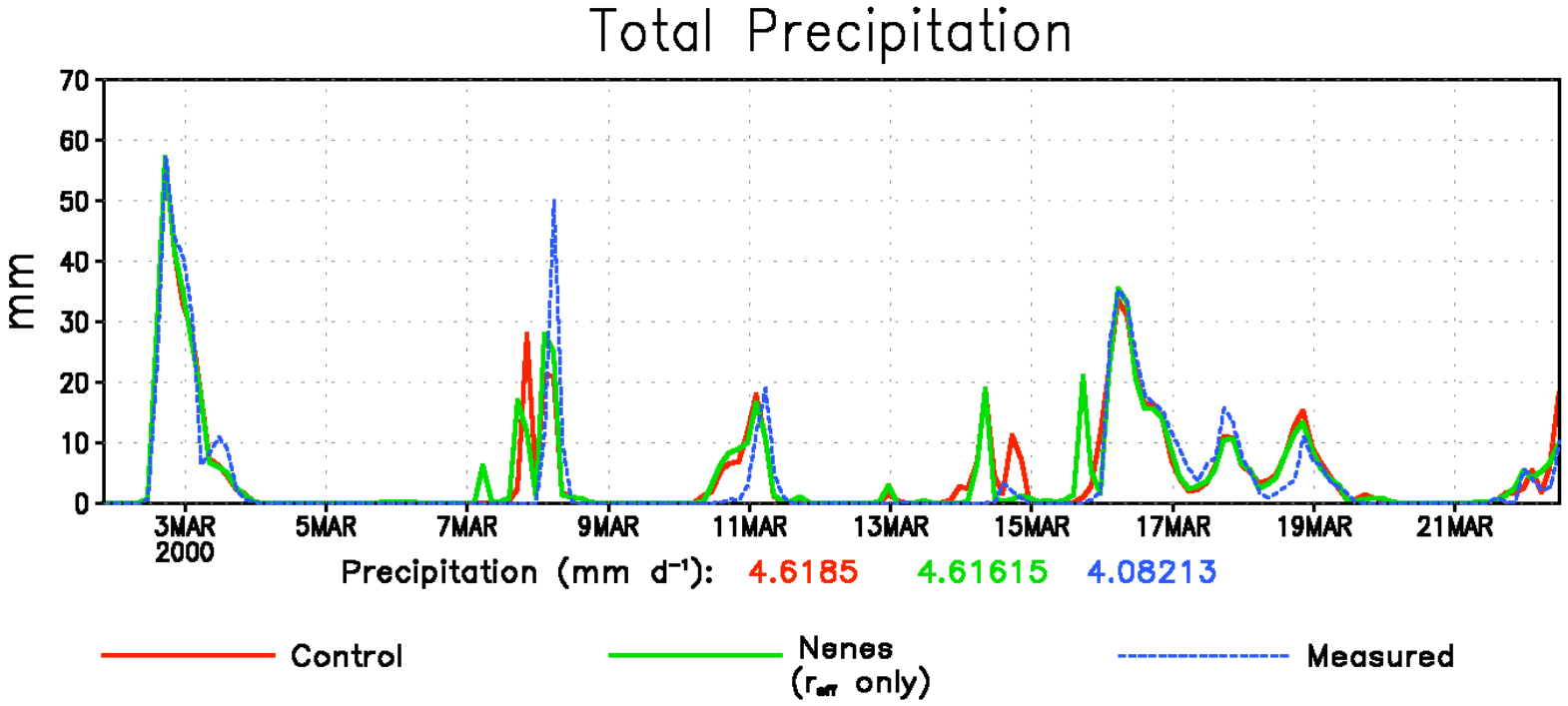
Total Precipitation
mm
70
60
50
40
30
20
10
0
3MAR
2000
5MAR
7MAR
9MAR
11MAR
13MAR
15MAR
17MAR
19MAR
21MAR
Precipitation (mm d⁻¹): 4.6185 4.61615 4.08213
Control
Nenes
(r_eff only)
Measured
ARM Case 4

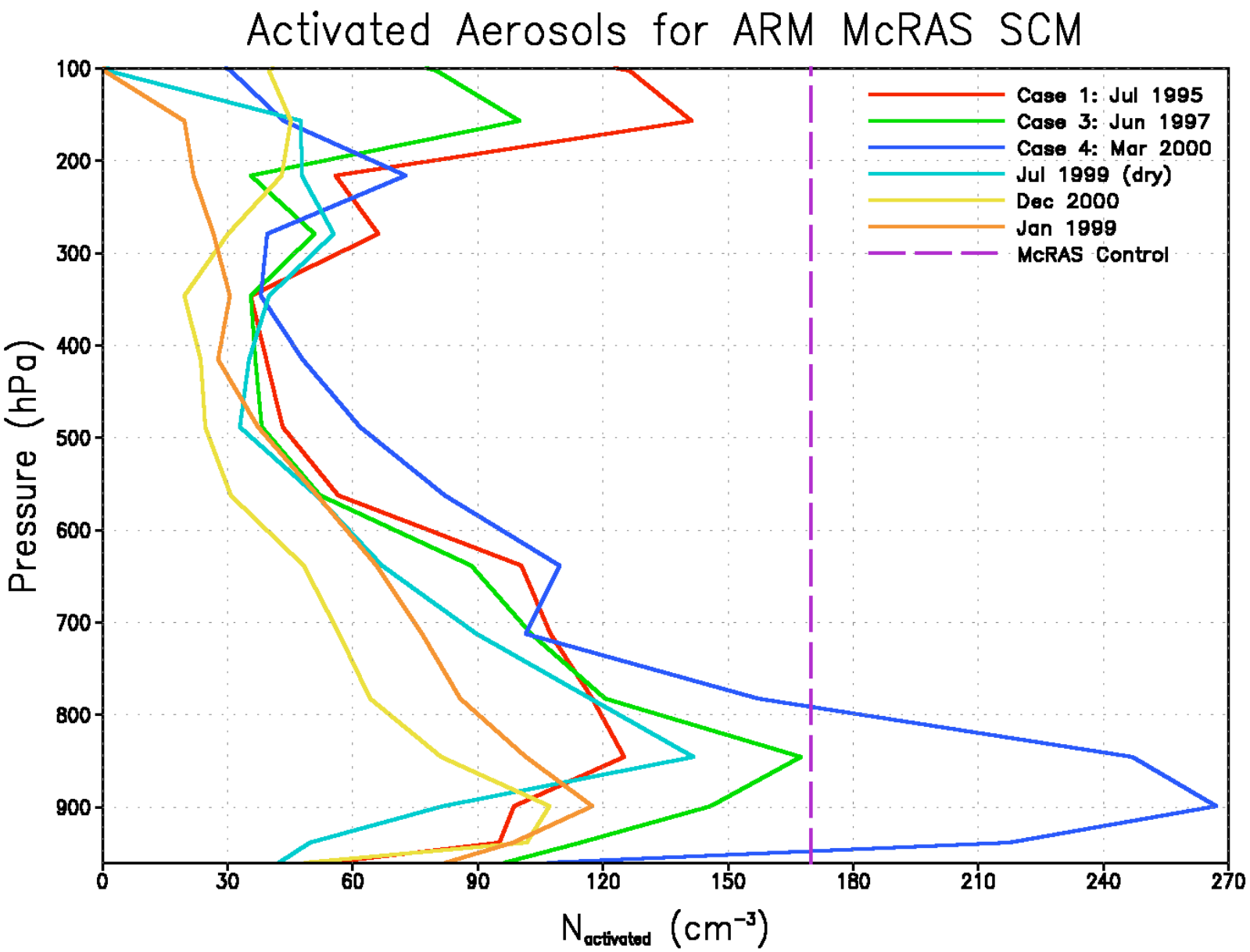
Activated Aerosols for ARM McRAS SCM
Pressure (hPa)
100
200
300
400
500
600
700
800
900
0
30
60
90
120
150
180
210
240
270
N activated (cm-3)
Case 1: Jul 1995
Case 3: Jun 1997
Case 4: Mar 2000
Jul 1999 (dry)
Dec 2000
Jan 1999
McRAS Control

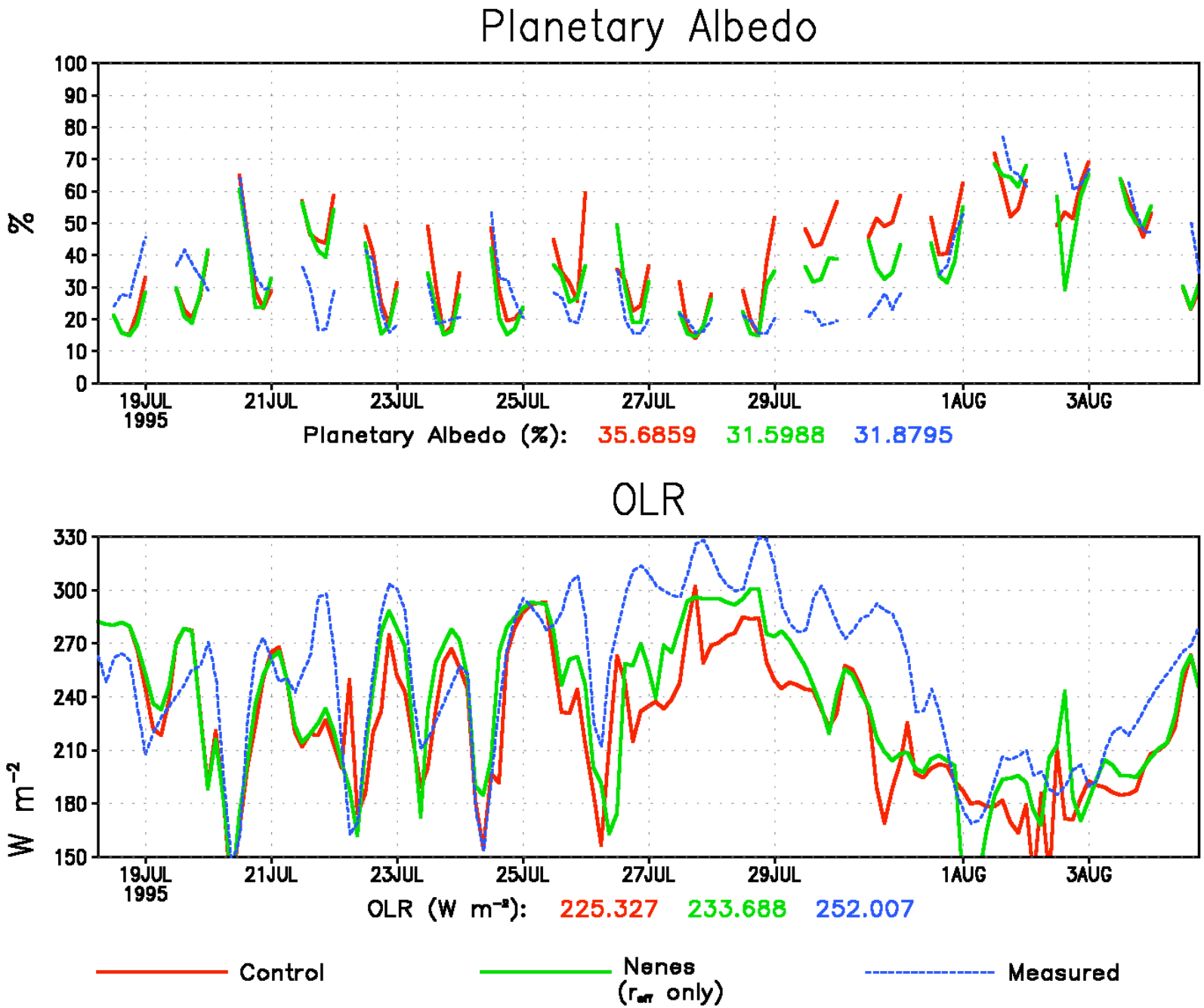
Planetary Albedo
100
90
80
70
60
50
40
30
20
10
0
%
19JUL
1995
21JUL
23JUL
25JUL
27JUL
29JUL
1AUG
3AUG
Planetary Albedo (%): 35.6859 31.5988 31.8795
OLR
330
300
270
240
210
180
150
W m⁻²
19JUL
1995
21JUL
23JUL
25JUL
27JUL
29JUL
1AUG
3AUG
OLR (W m⁻²): 225.327 233.688 252.007
Control
Nenes
(r_eff only)
Measured
ARM Case 1

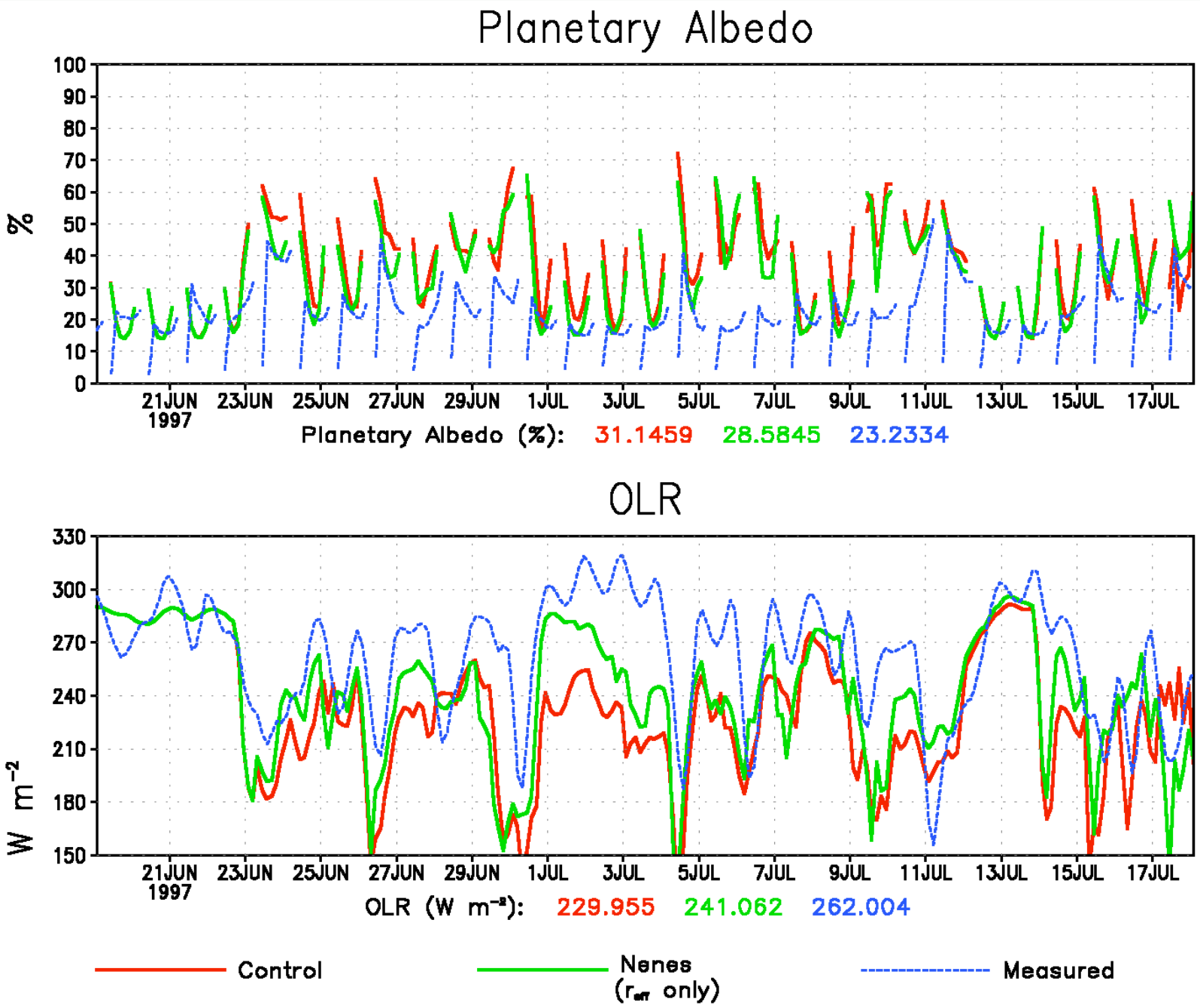
Planetary Albedo
100
90
80
70
60
50
40
30
20
10
0
%
21JUN 1997
23JUN
25JUN
27JUN
29JUN
1JUL
3JUL
5JUL
7JUL
9JUL
11JUL
13JUL
15JUL
17JUL
Planetary Albedo (%): 31.1459 28.5845 23.2334
OLR
330
300
270
240
210
180
150
W m⁻²
OLR (W m⁻²): 229.955 241.062 262.004
Control
Nenes
(r_eff only)
Measured
ARM Case 3

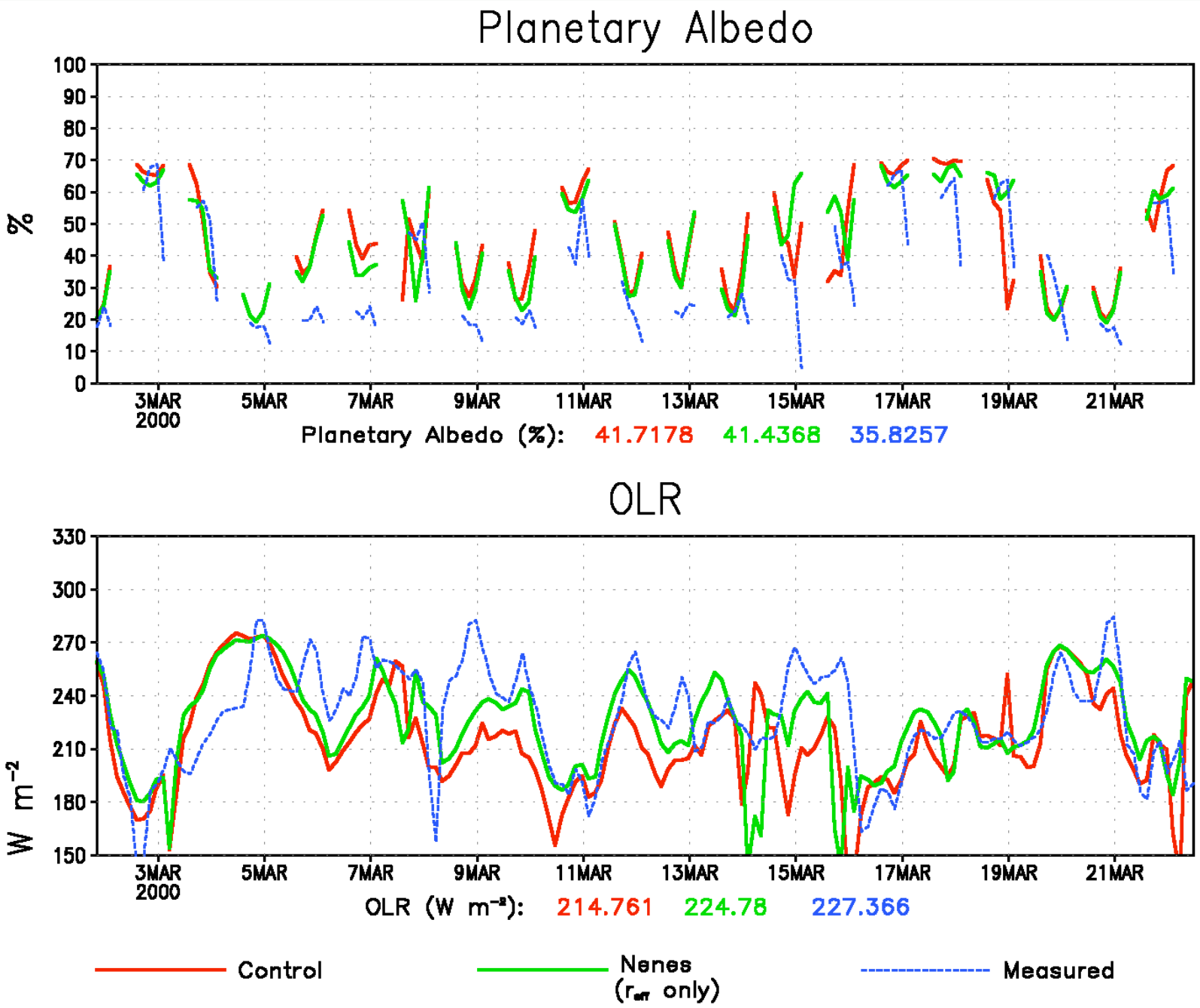
Planetary Albedo
%
100
90
80
70
60
50
40
30
20
10
0
3MAR 2000
5MAR
7MAR
9MAR
11MAR
13MAR
15MAR
17MAR
19MAR
21MAR
Planetary Albedo (%): 41.7178 41.4368 35.8257
OLR
W m⁻²
330
300
270
240
210
180
150
OLR (W m⁻²): 214.761 224.78 227.366
Control
Nenes (r_eff only)
Measured
ARM Case 4

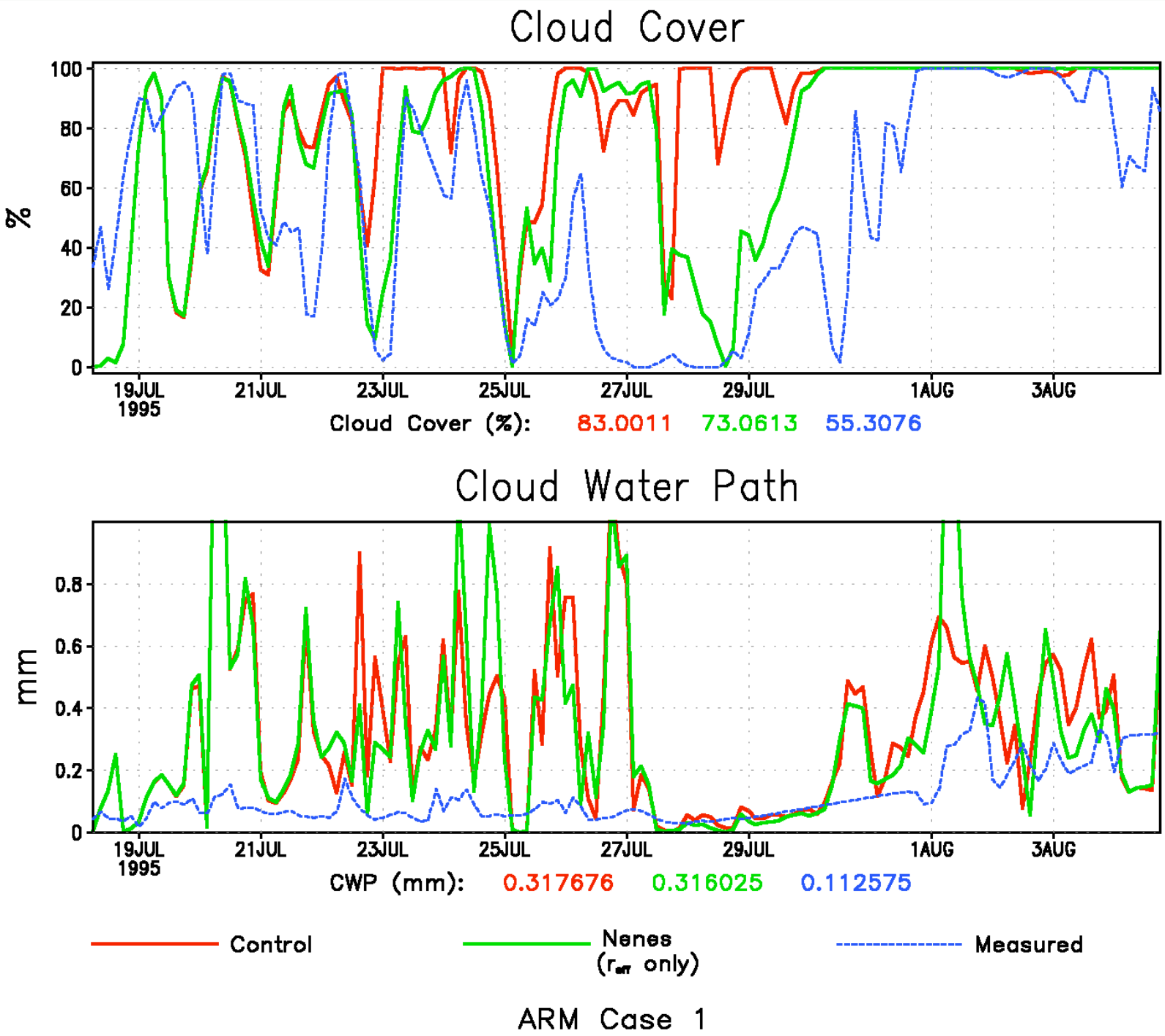
Cloud Cover
%
100
80
60
40
20
0
19JUL
1995
21JUL
23JUL
25JUL
27JUL
29JUL
1AUG
3AUG
Cloud Cover (%): 83.0011 73.0613 55.3076
Cloud Water Path
mm
0.8
0.6
0.4
0.2
0
CWP (mm): 0.317676 0.316025 0.112575
Control
Nenes
(r_eff only)
Measured
ARM Case 1

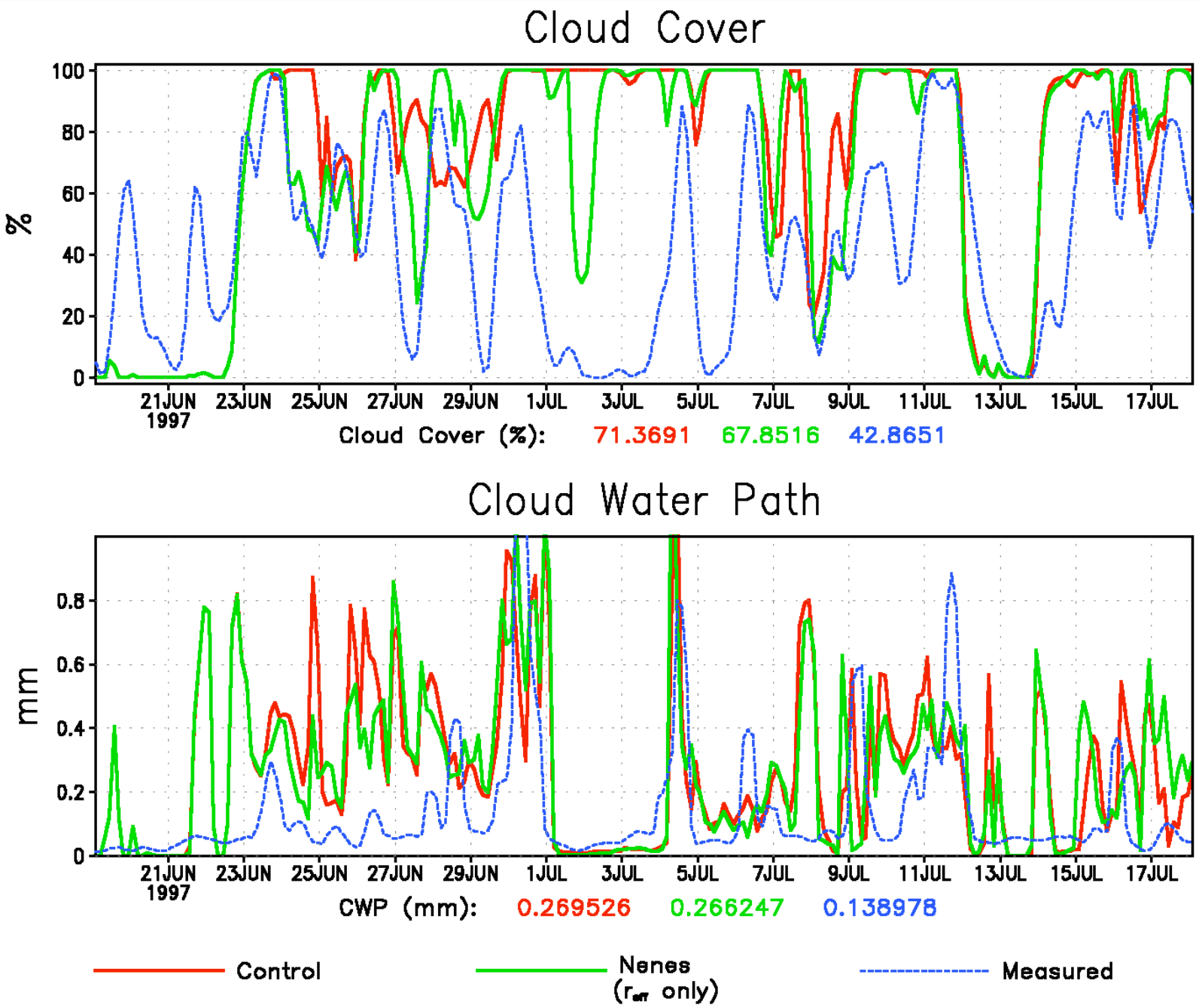
Cloud Cover
100
80
60
40
20
0
%
21JUN 1997
23JUN
25JUN
27JUN
29JUN
1JUL
3JUL
5JUL
7JUL
9JUL
11JUL
13JUL
15JUL
17JUL
Cloud Cover (%): 71.3691 67.8516 42.8651
Cloud Water Path
0.8
0.6
0.4
0.2
0
mm
21JUN 1997
23JUN
25JUN
27JUN
29JUN
1JUL
3JUL
5JUL
7JUL
9JUL
11JUL
13JUL
15JUL
17JUL
CWP (mm): 0.269526 0.266247 0.138978
Control
Nenes (r_{eff} only)
Measured
ARM Case 3

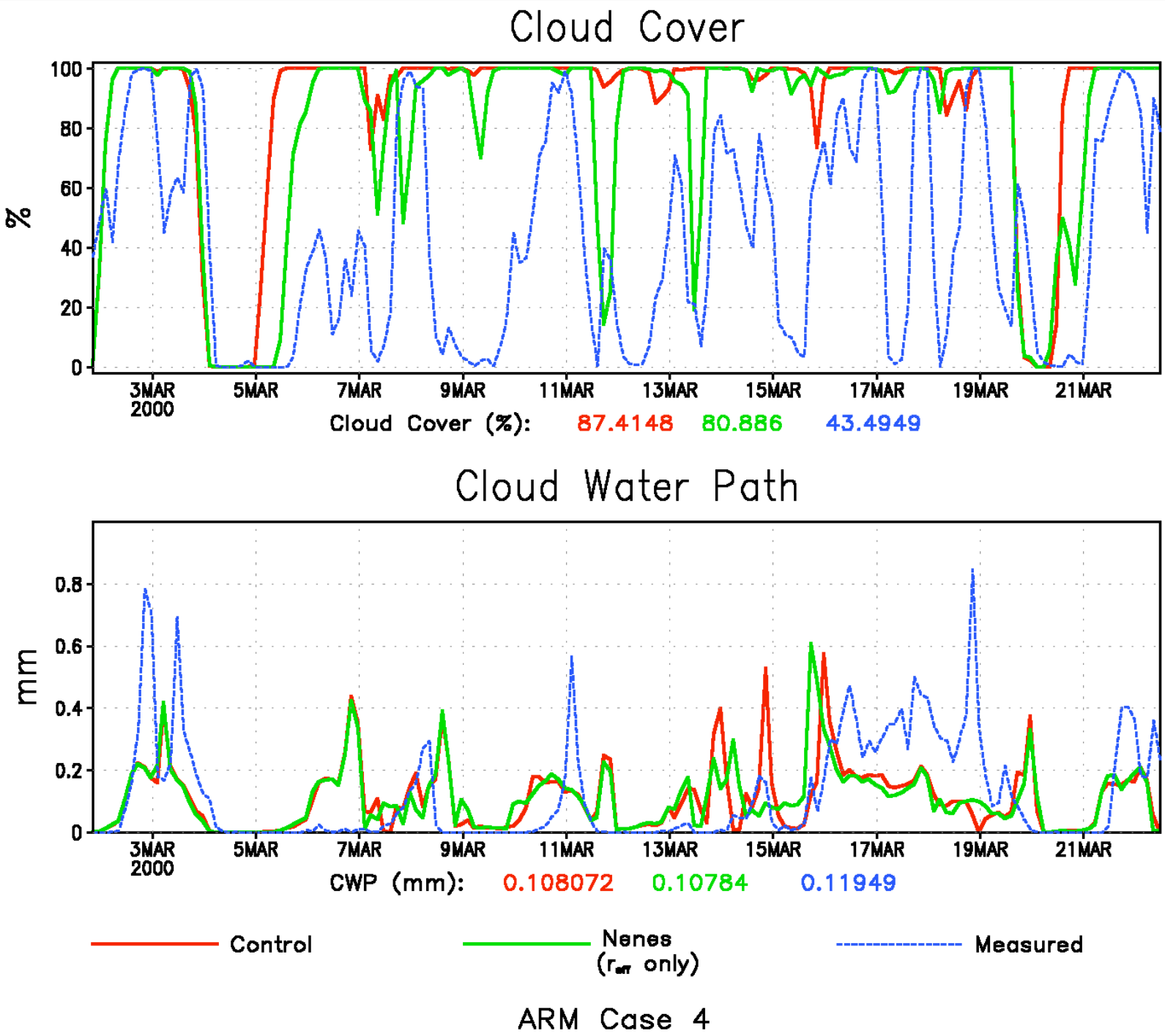
Cloud Cover
100
80
60
40
20
0
%
3MAR
2000
5MAR
7MAR
9MAR
11MAR
13MAR
15MAR
17MAR
19MAR
21MAR
Cloud Cover (%): 87.4148 80.886 43.4949
Cloud Water Path
0.8
0.6
0.4
0.2
0
mm
CWP (mm): 0.108072 0.10784 0.11949
Control
Nenes
(r_{eff} only)
Measured
ARM Case 4

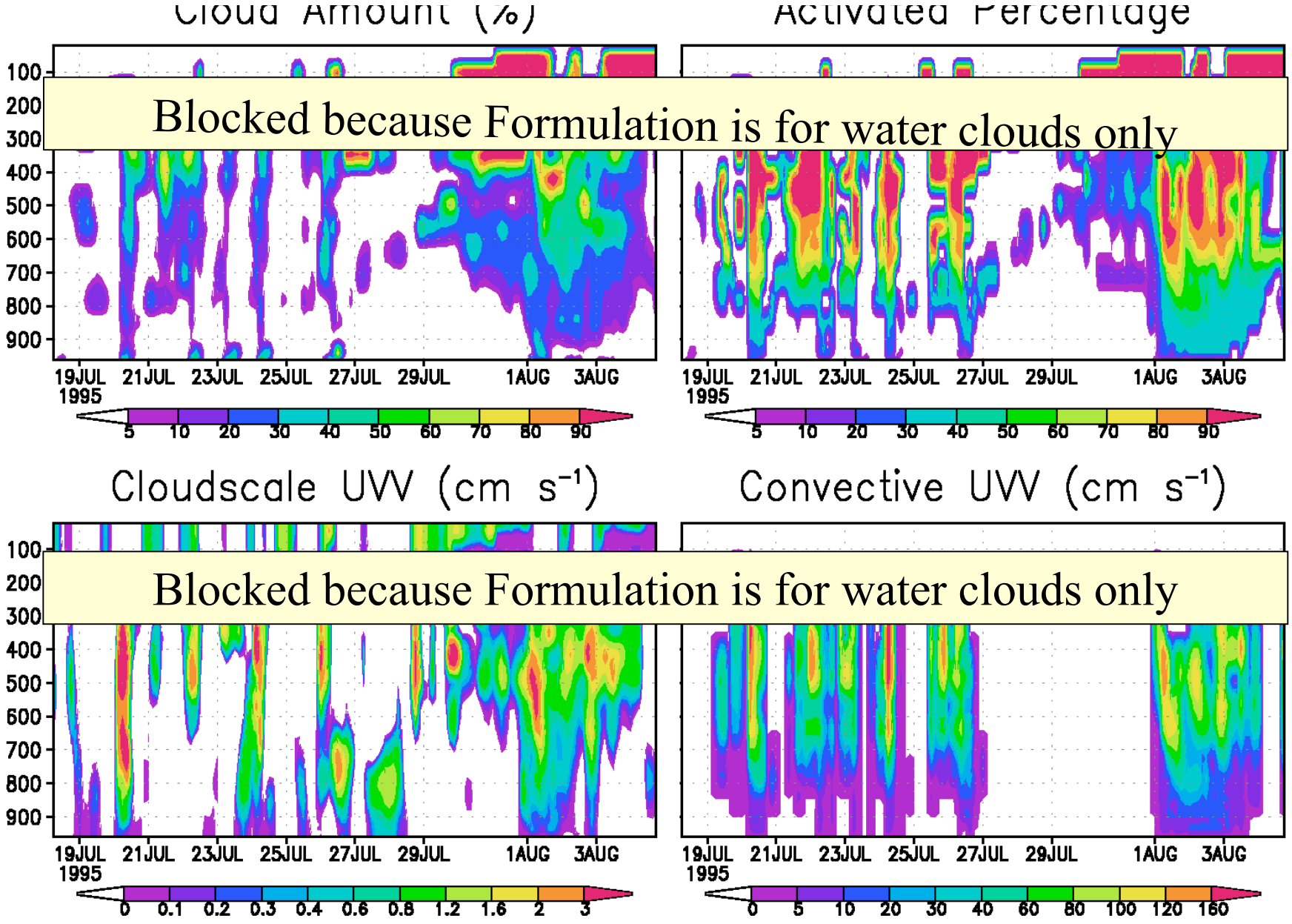

ARM Case 1: McRAS SCM simulation with Nenes aerosol activation

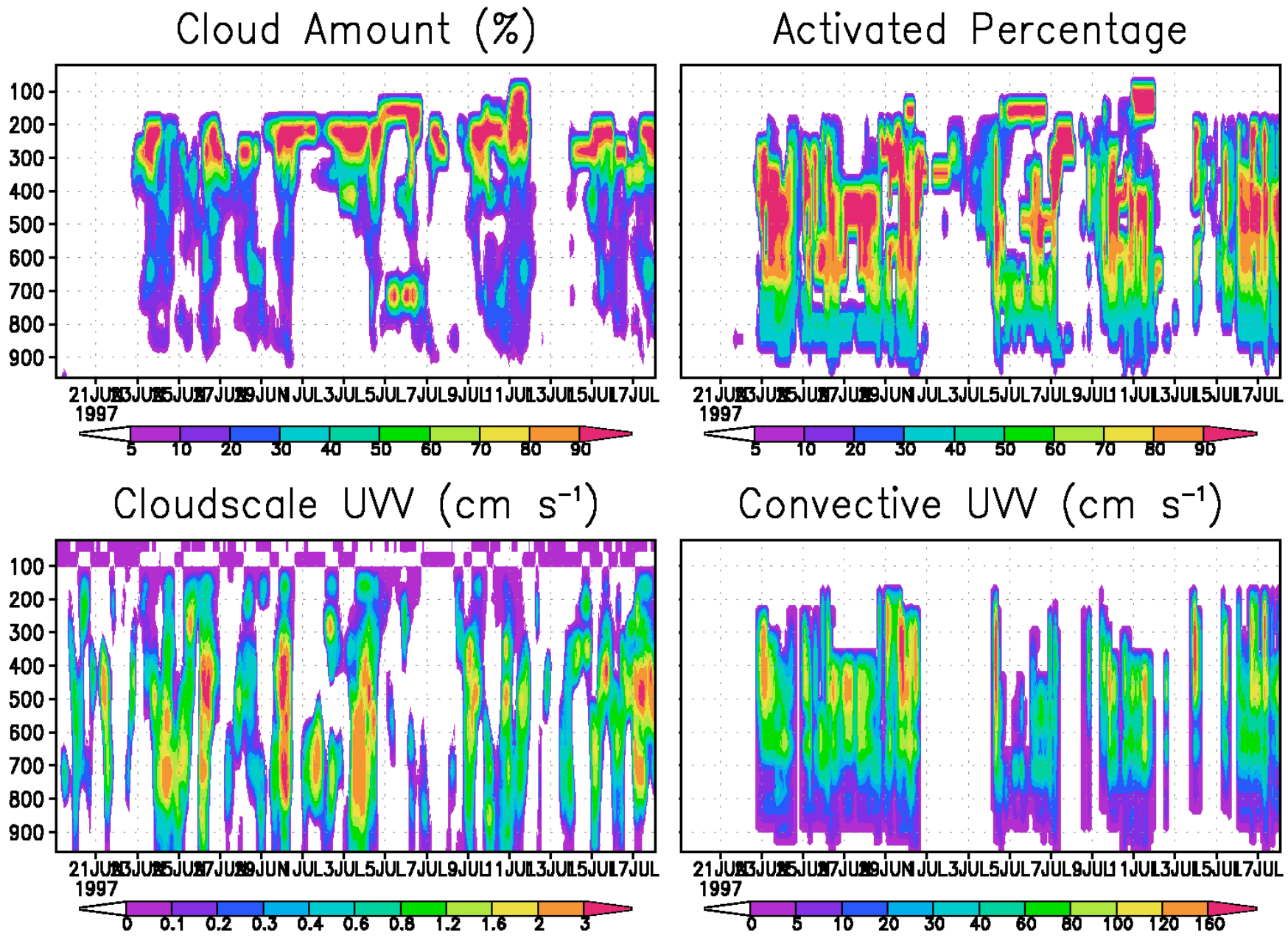

ARM Case 3: McRAS SCM simulation with Nenes aerosol activation

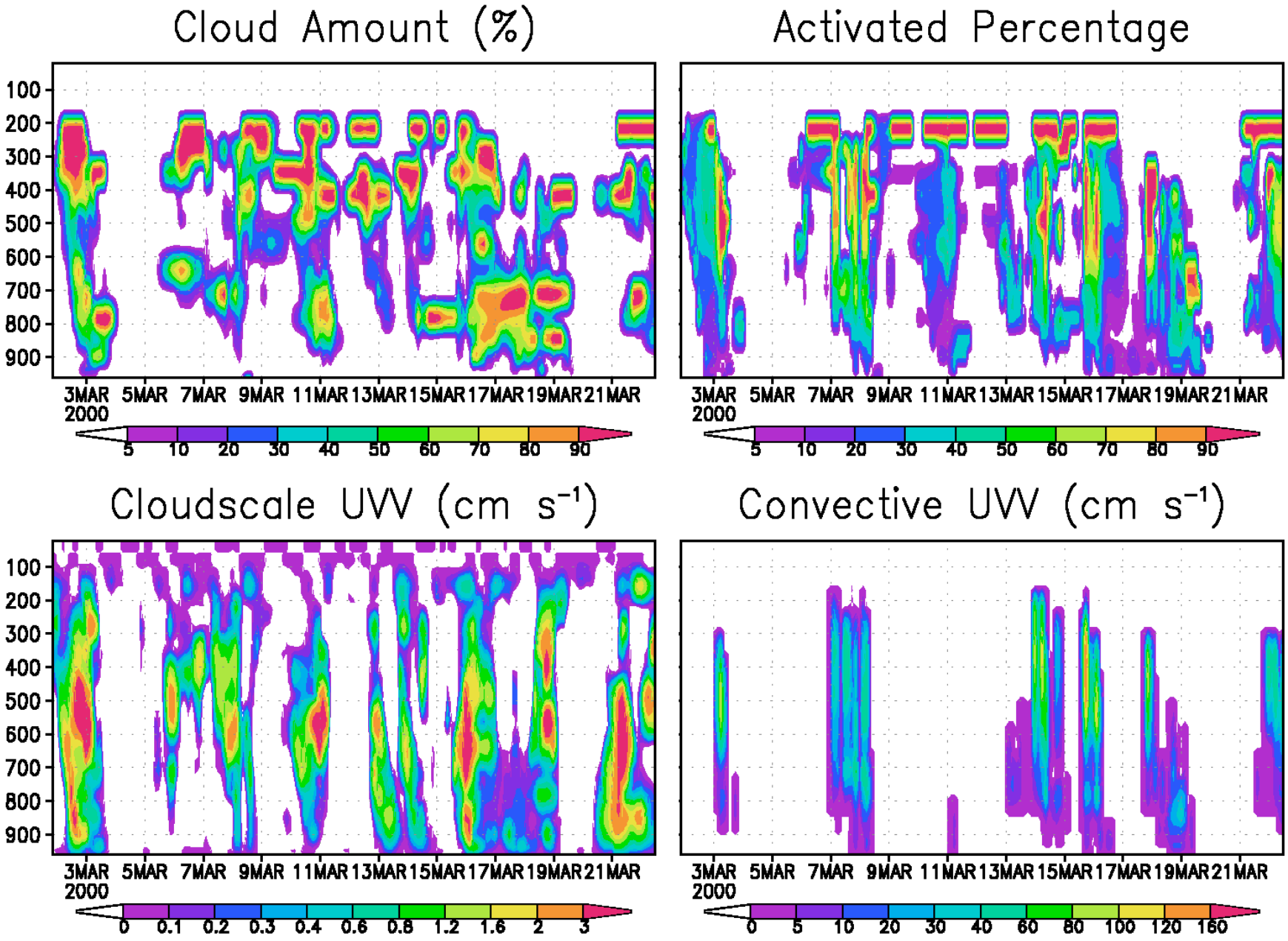

ARM Case 4: McRAS SCM simulation with Nenes aerosol activation

Conclusions

1. Only sulfate aerosols were chosen to interact with clouds in this semi-empirical evaluation (AC-MIP recommendation) ; however, we find huge cloud water differences over North Pacific and Atlantic regions in the response. This alters the radiation balance, even the cooling in the polar regions. Regardless of its importance for global warming, CDNCs and DSDs are potentially important for reducing a GCMs cloud-radiation interaction biases.
2. The ITCZ and rainfall was also affected in the AC-MIP simulation; over the polluted subcontinents of India and China, JJA/monsoon rainfall was reduced. With full feedbacks in a coupled model, the affect is likely to be much more dramatic. At this time, the changes in the thermal forcing is so much model-to-model dependant (also noted in our auto-conversion formulations test), this area needs far more attention and concerted research than

Conclusions-Continued

3. Nenes and Seinfeld (2003) aerosol activation is based on first principles (i.e., without proverbial tuning) . McRAS offers great promise particularly because McRAS provides sub-grid scale vertical motion fields and rainfall production microphysics that is prognostic. We have it fully coupled to McRAS and could easily run sensitivity experiments.
4. Some of the leading and recently published parameterizations of CDNCs (including Nenes) still assume DSD/Effective radius. We propose to infer DSDs from Population Splitting assumption of Nenes and **Köhler's** Equation.
5. Clearly aerosol-ice microphysics has been poorly developed for model-applications; it must get due attention. ***Nenes is working on it and promises to provide its timely inclusion.*** We hope to continue our collaboration with Nenes on this very important problem.

END TALK

END TALK

END TALK

END TALK

Overview of the different aerosol indirect effects*

*influence of natural and such as dust and biogenic aerosols and sea-salts is not depicted in this illustration

(Lohman et al. 2004)

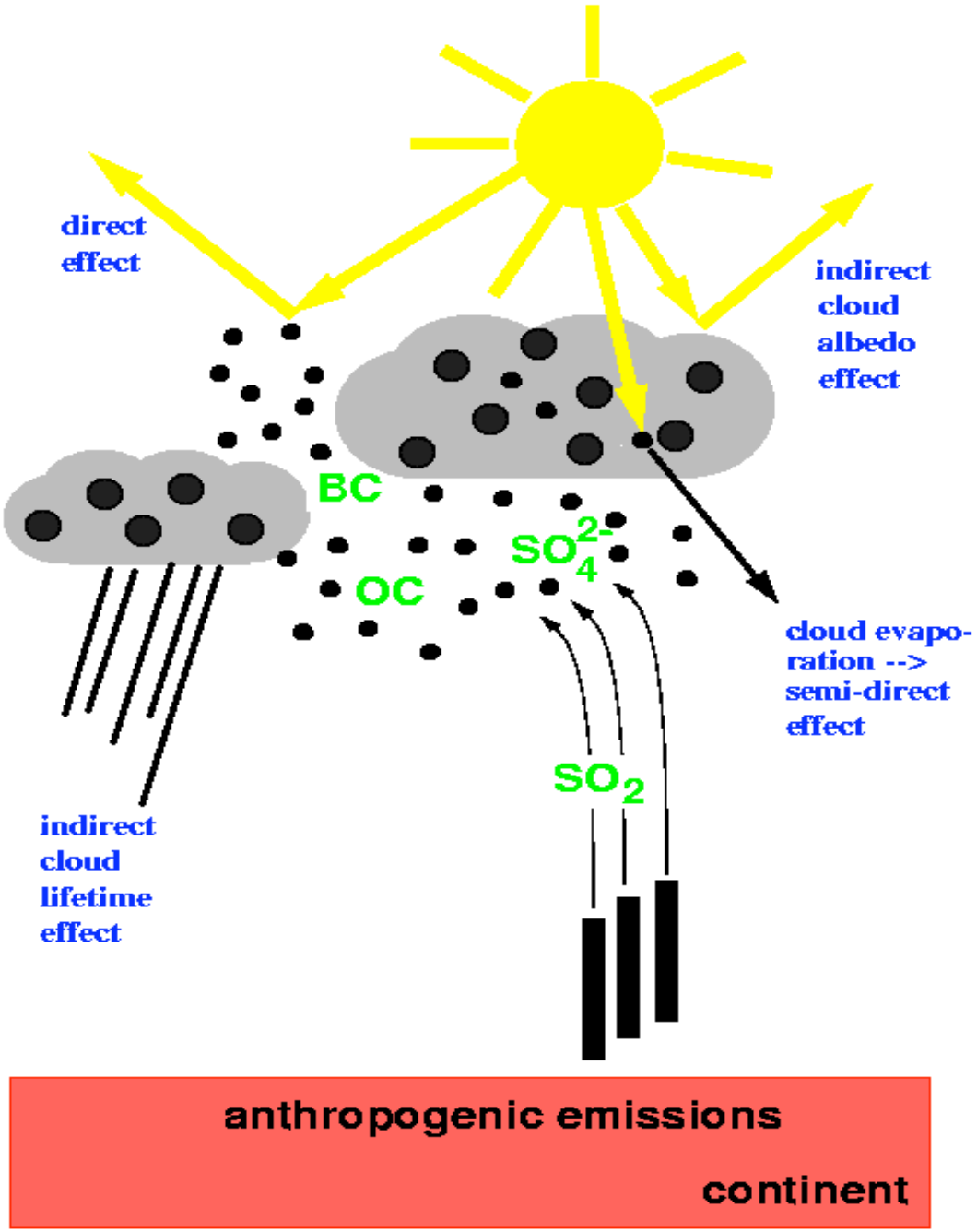

Microphysical Pathways

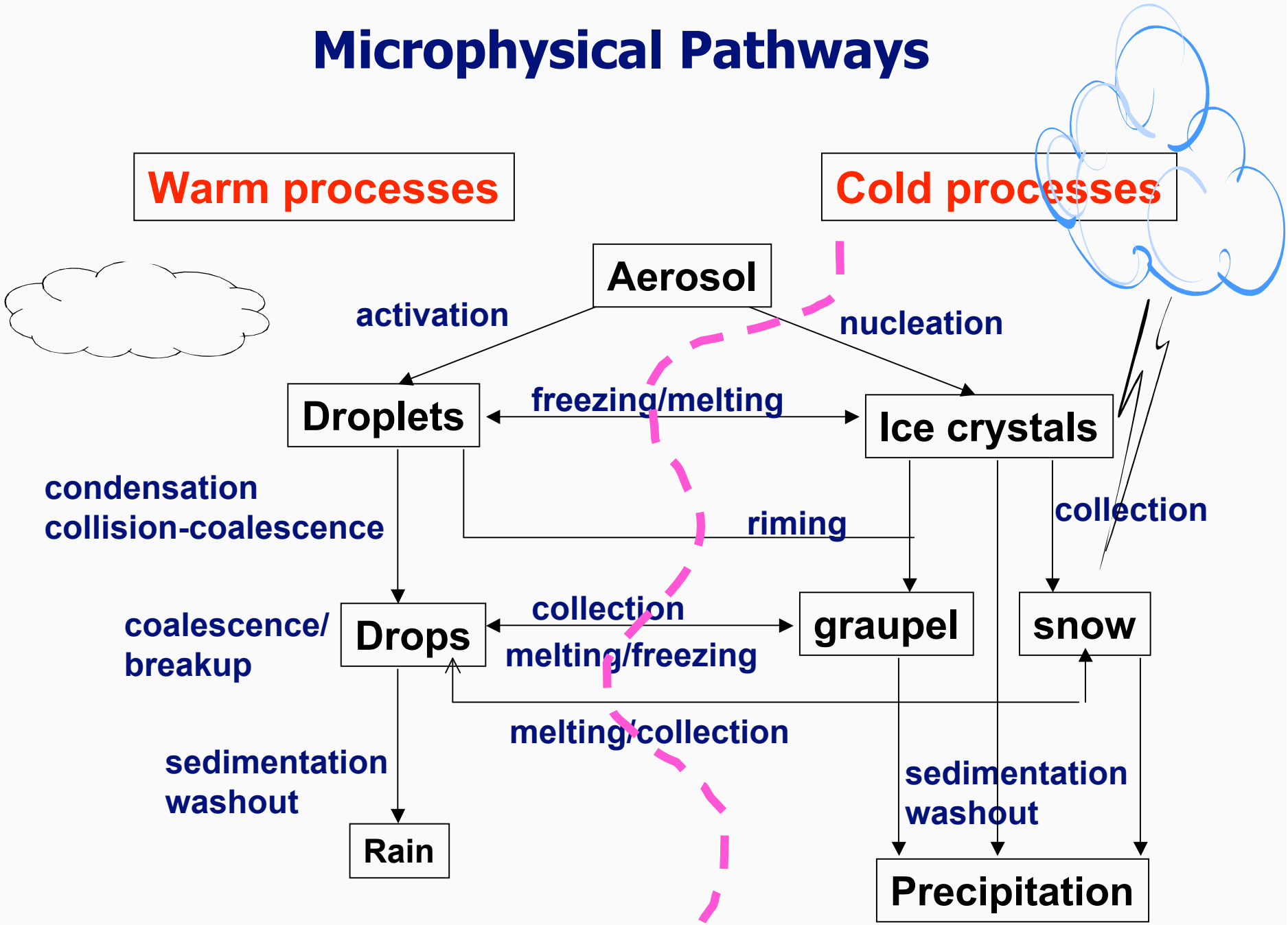

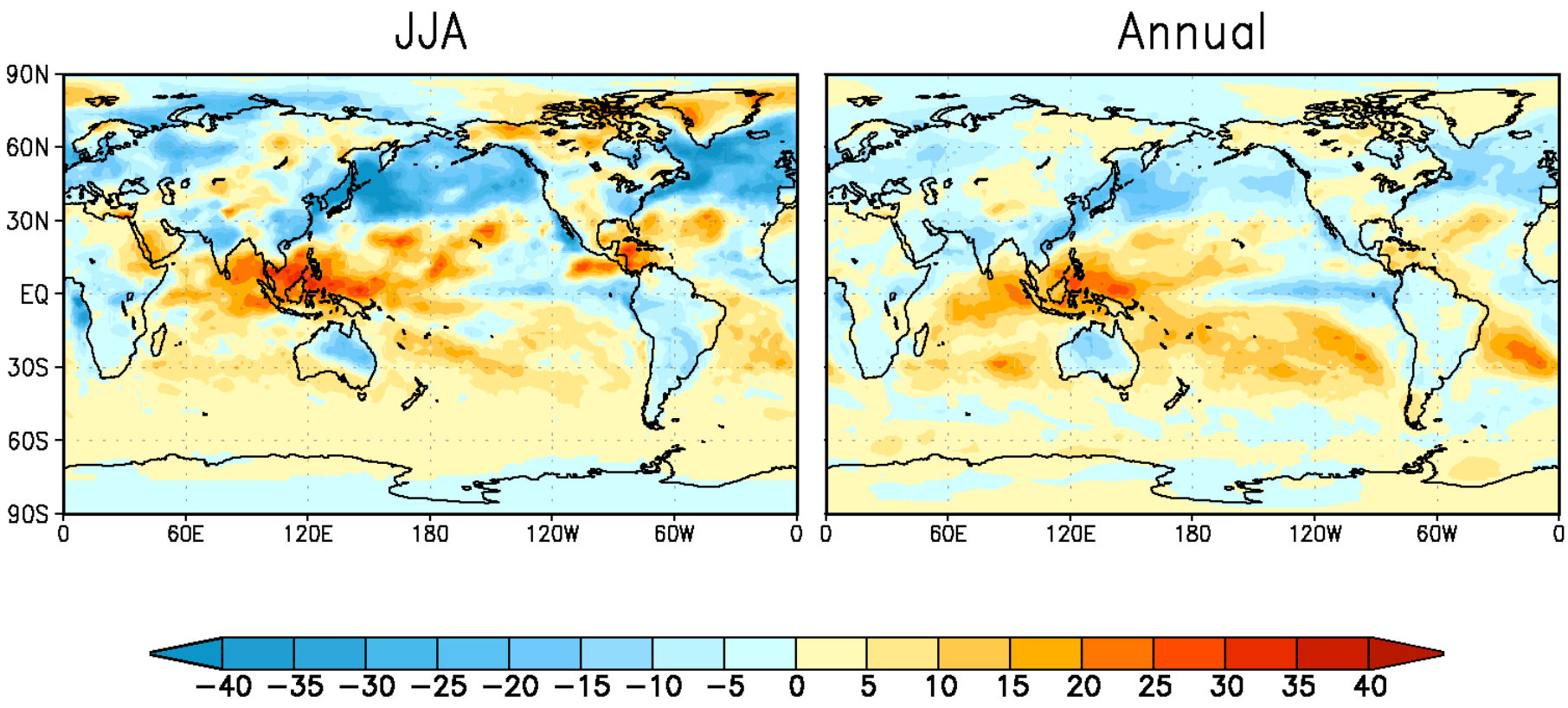

Surface incident shortwave radiation (W m^{-2}) difference from Control.

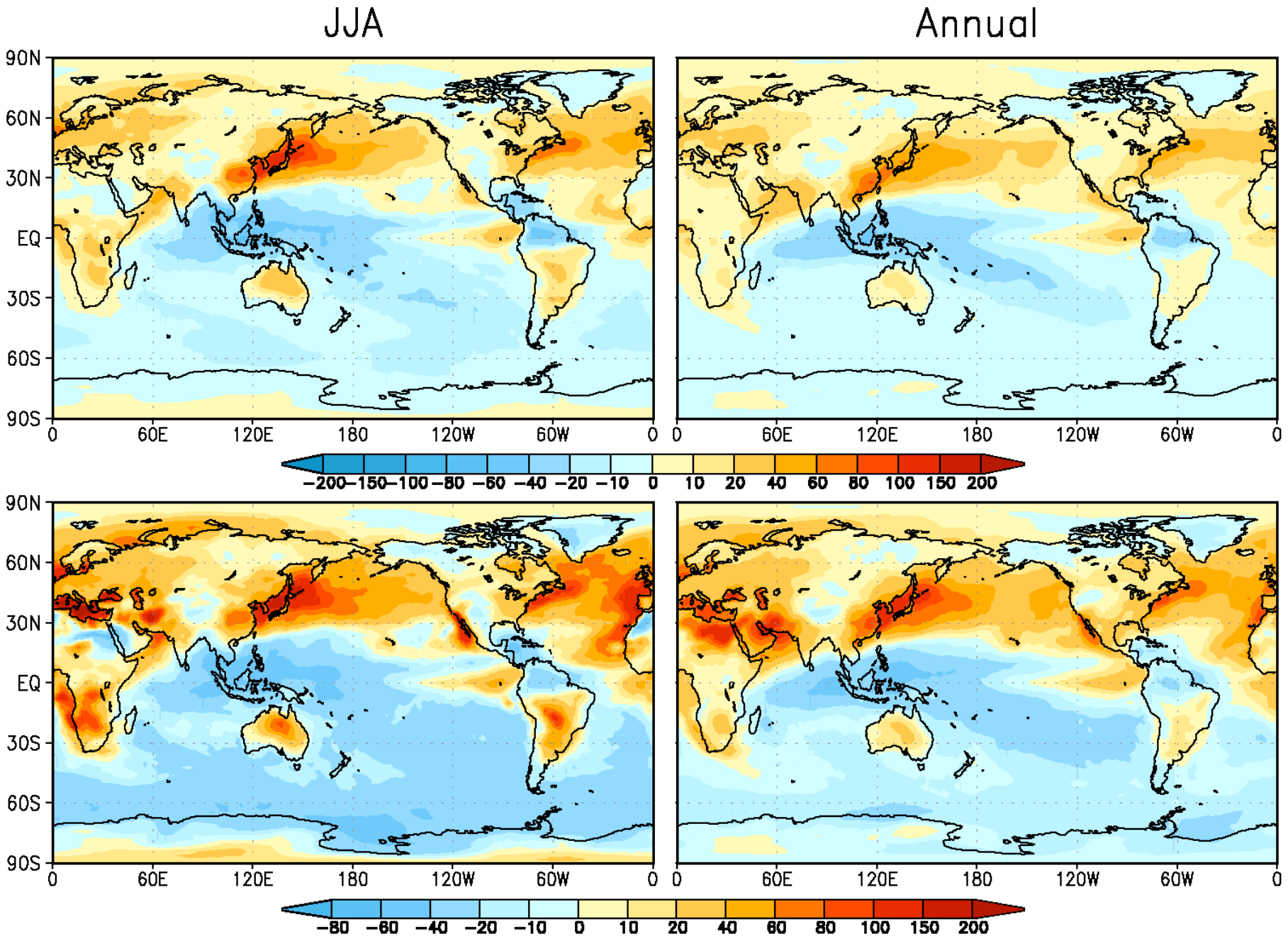

Column optical thickness difference from Control (top) and percent difference (bottom)

Highlights

1. Both the direct and indirect effects of aerosols can be significant.
2. The indirect effect has the most uncertainty associated to it because aerosol-cloud coupling has either been ignored or poorly estimated in almost all GCMs.
3. There is growing body of evidence that inadequate aerosol treatments can lead to large biases and make our GCMs ill-suited for predicting anthropogenically forced climate-change.
4. Some preliminary results from GCM and single column model (SCM) simulations will be shown. Such exercises pave the way toward reducing the uncertainty in simulating the indirect effect of aerosols on clouds and cloud-radiative forcing of the simulated Earth-Atmosphere system.

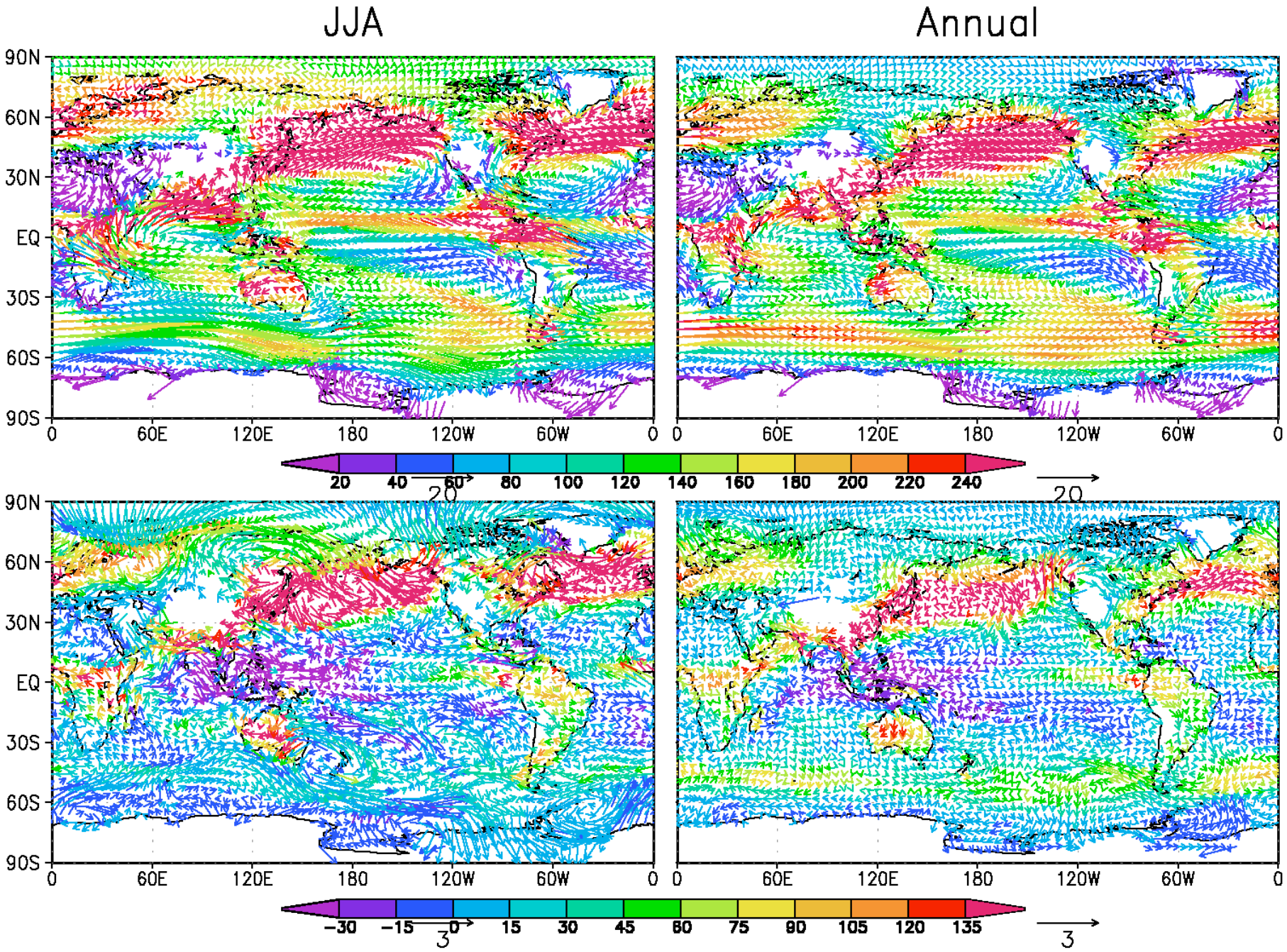

850hPa winds (top) and difference from Control (bottom). Color represents column cloud water path (g m^{-2}).

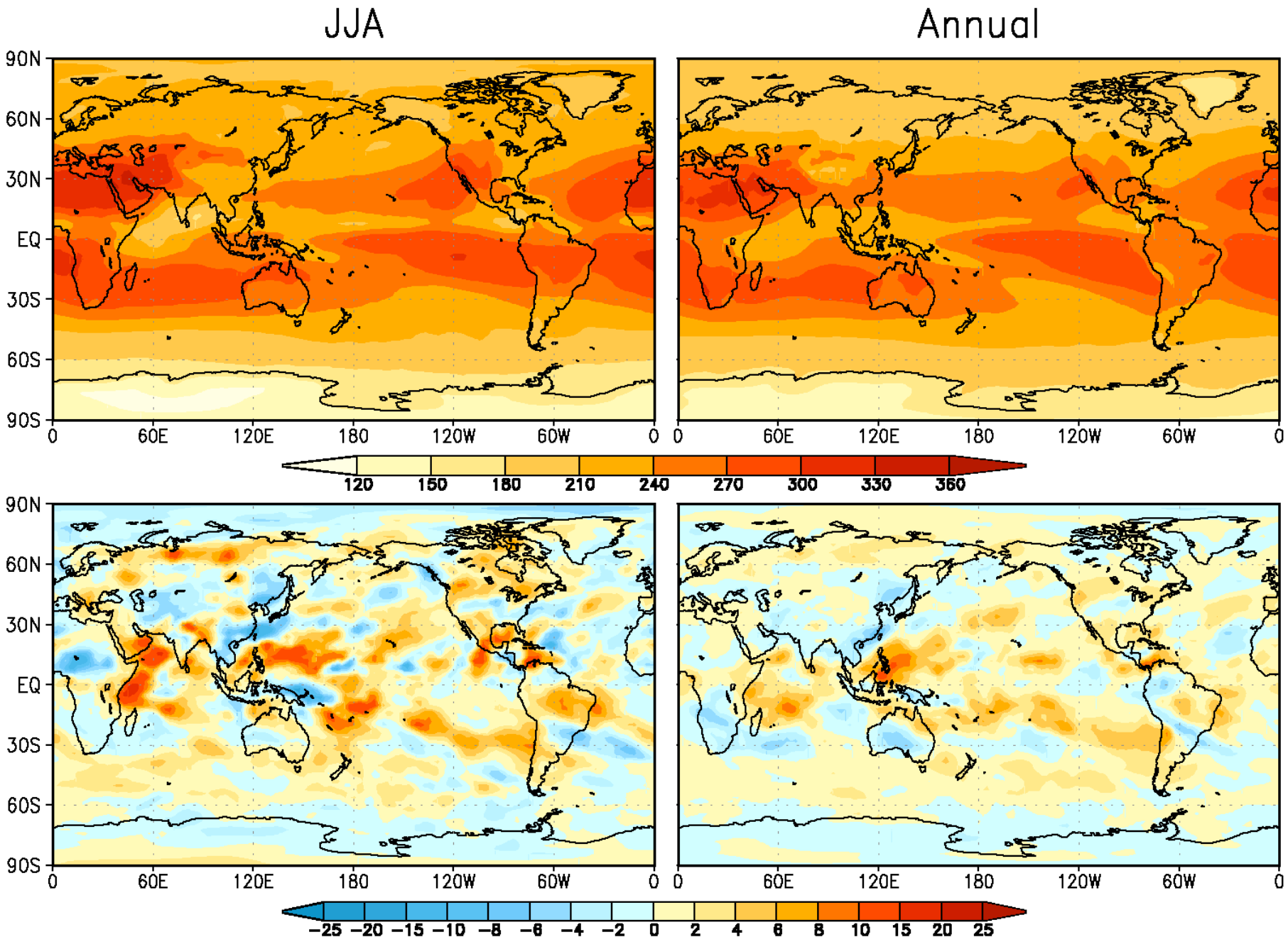

Outgoing longwave radiation (W m^{-2}) (top) and difference from Control (bottom).

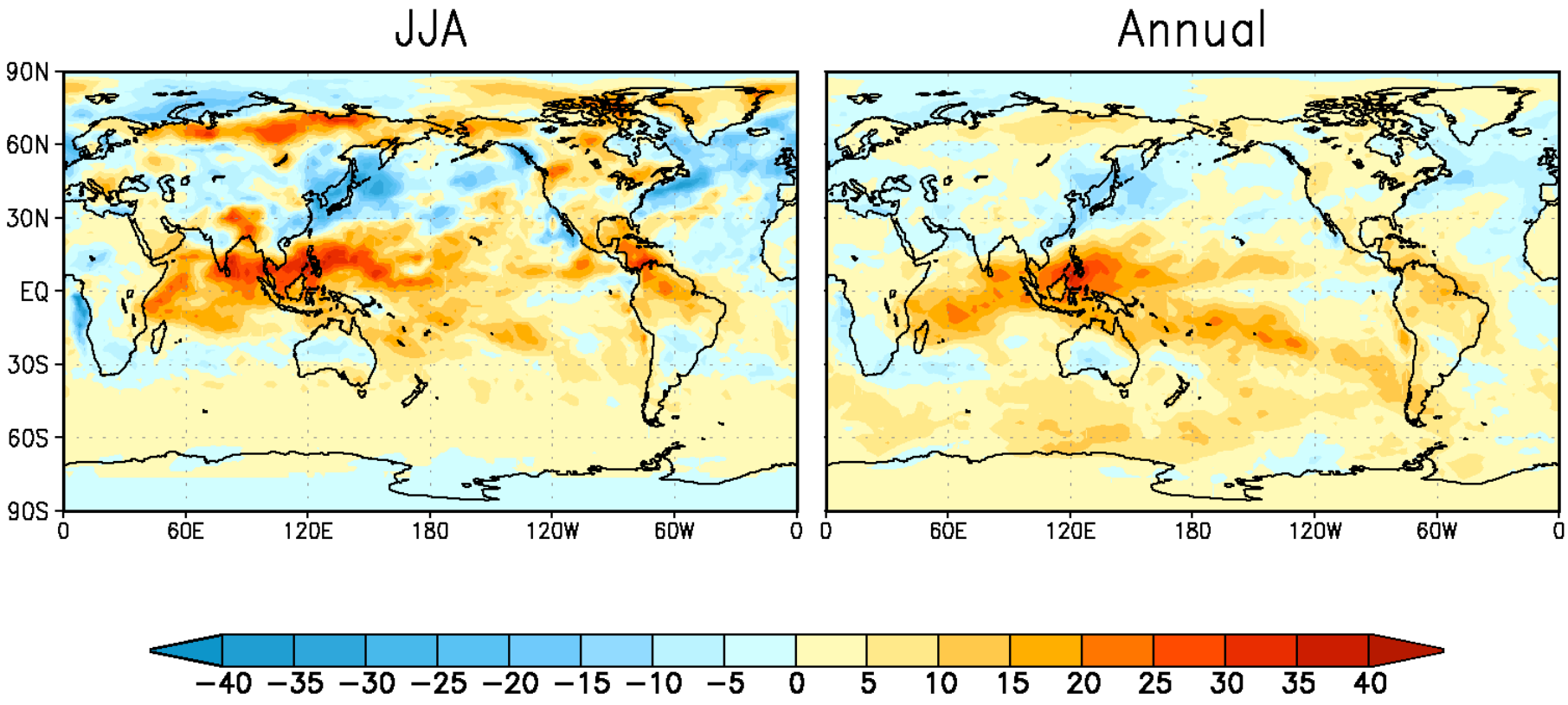

Surface incident shortwave radiation (W m^{-2}) difference from Control.

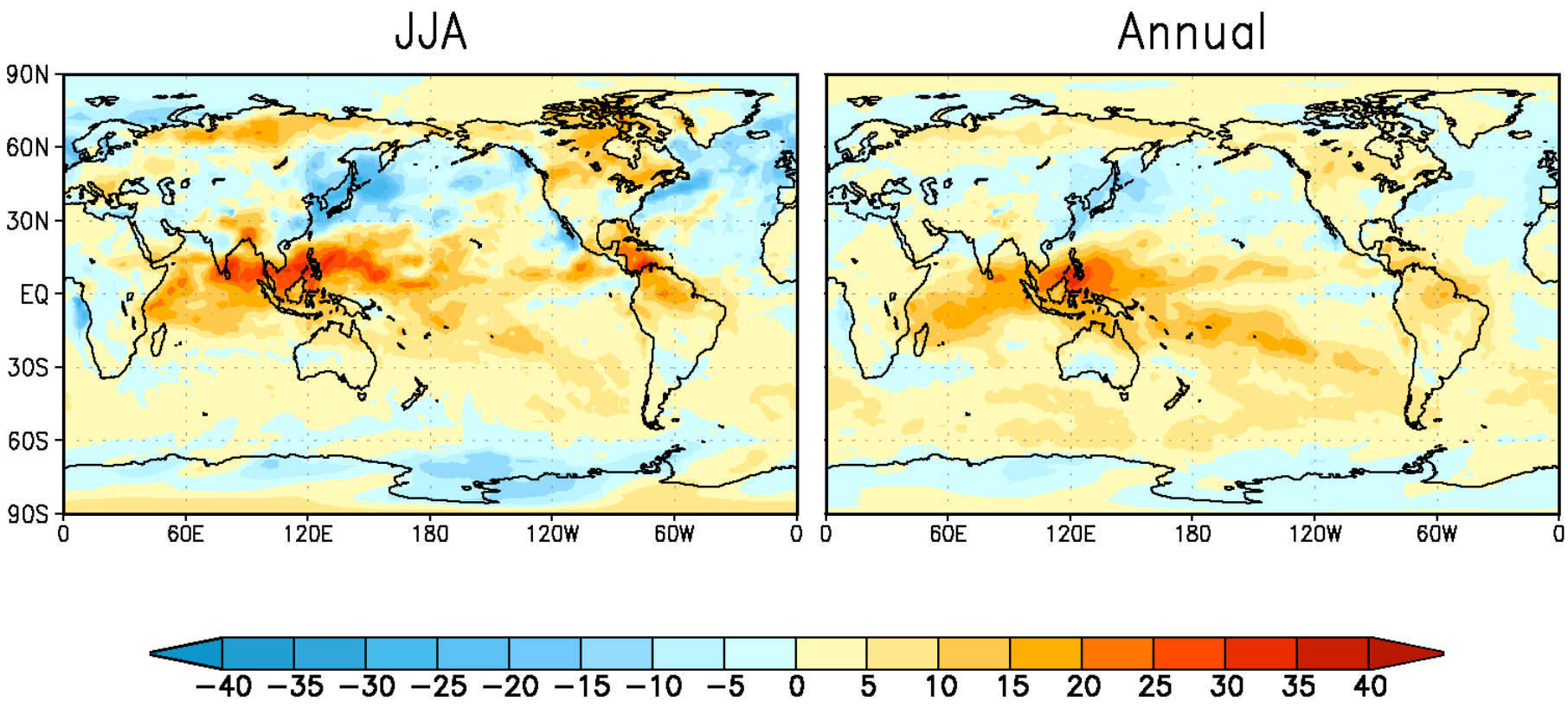

Surface net radiative forcing (W m^{-2}) difference from Control.

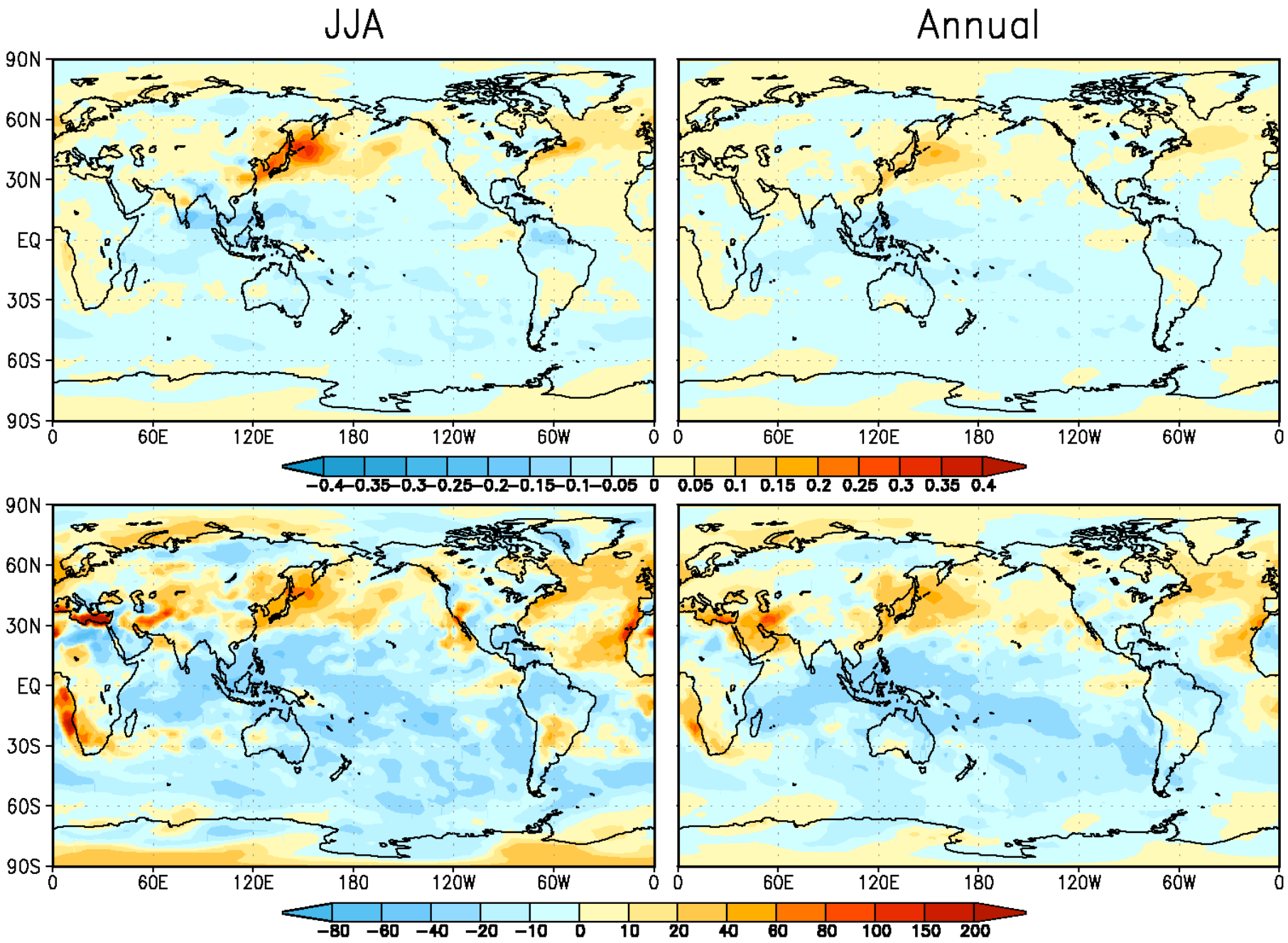

Column cloud water (kg m^{-2}) difference from Control (top) and percent difference (bottom)

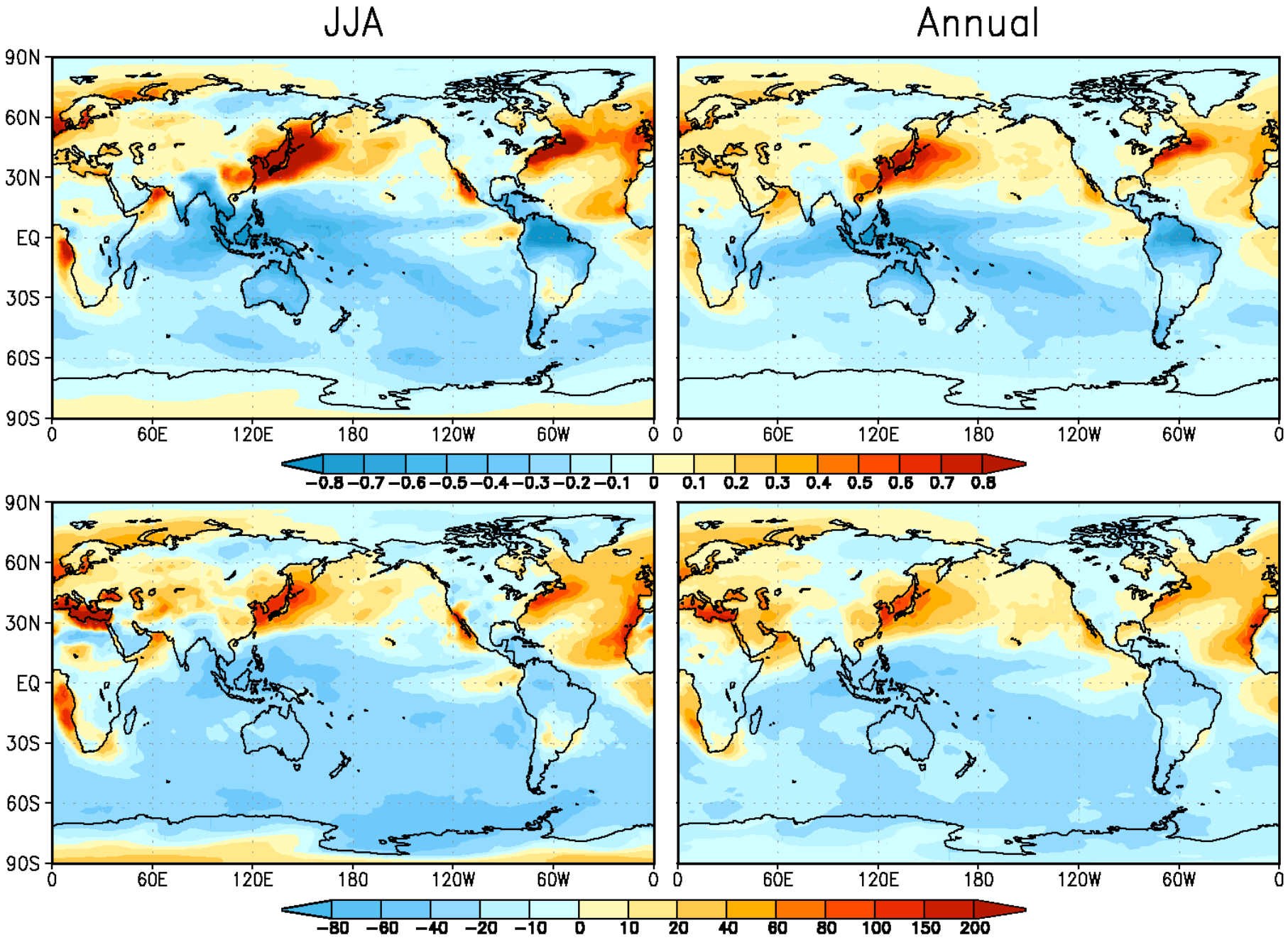

Column optical thickness difference from Control (top) and percent difference (bottom)

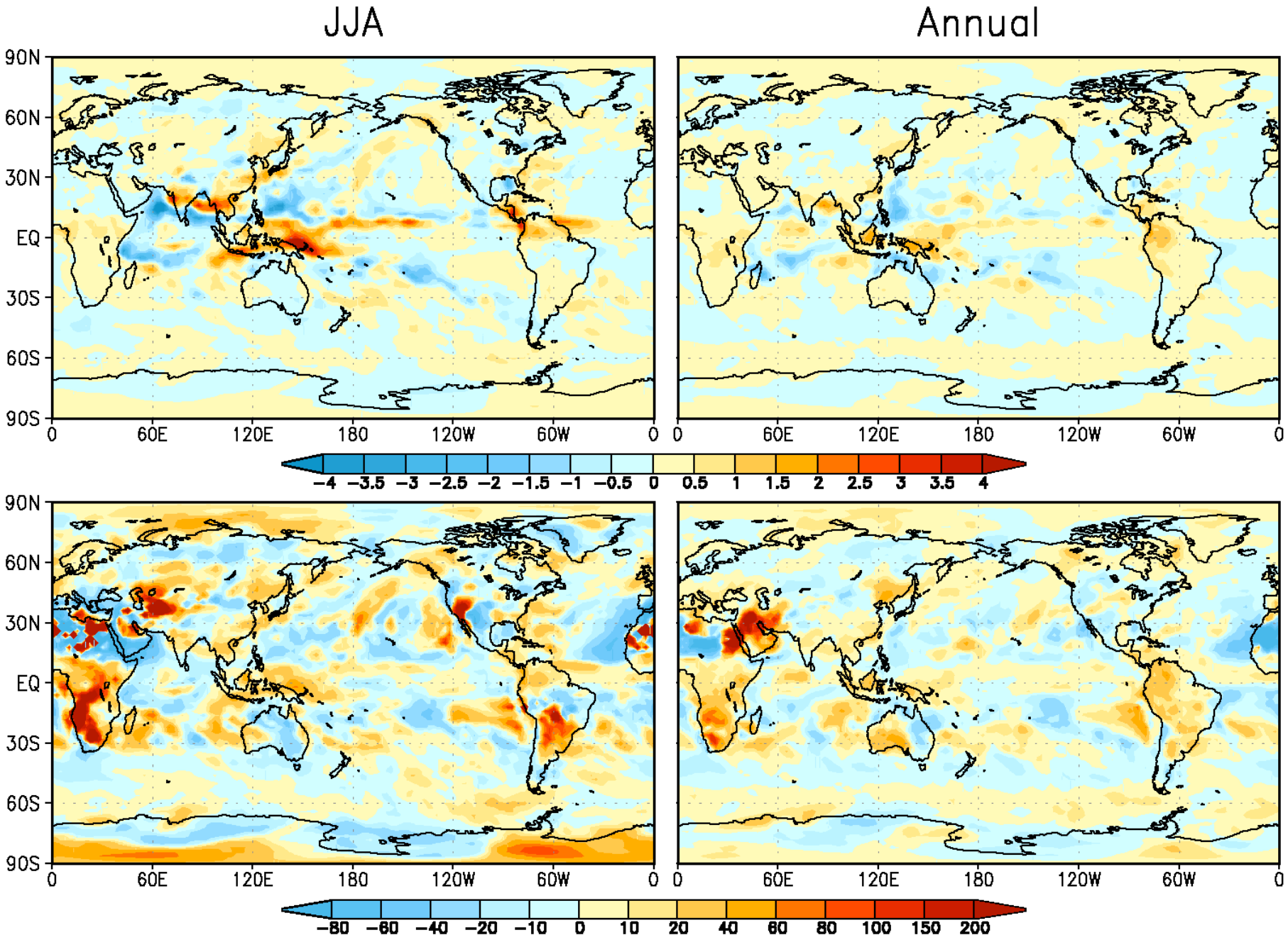

Precipitation (mm d^{-1}) difference from Control (top) and percent difference (bottom)

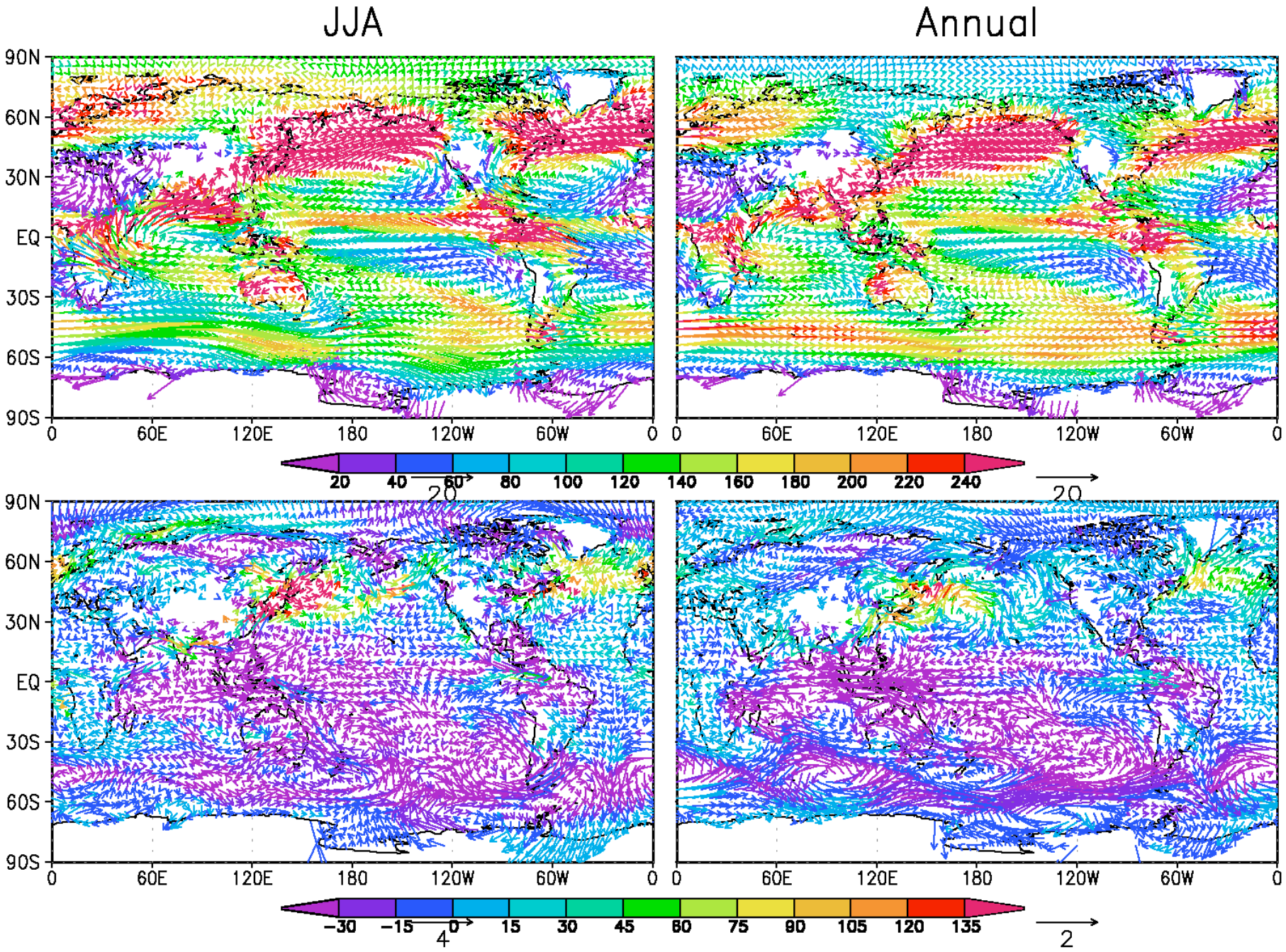

850hPa winds (top) and difference from Control (bottom). Color represents column cloud water path (g m^{-2}).

JJA: GOCART Aerosol Optical Thickness (left) cloud-water path (middle) and condensation heating (right)